CHAPTER

# 4

# Earth-abundant electrocatalysts for sustainable energy conversion

*Chong-Yong Lee*[a], *John P. Bullock*[b], *and*
*Gordon G. Wallace*[a]

**[a]ARC Centre of Excellence for Electromaterials Science, Intelligent Polymer Research Institute, AIIM, Innovation Campus, University of Wollongong, Wollongong, NSW, Australia, [b]Division of Natural Science and Mathematics, Bennington College, Bennington, Vermont, United States**

## 1 Introduction

The release of anthropogenic greenhouse gases into the atmosphere, primarily from the heavy reliance on fossil fuels to drive the world economy, has resulted in the imminent threats of global warming and climate change, rising sea levels, ocean acidification, melting of glaciers and permafrost, and more frequent and severe weather patterns [1, 2]. Atmospheric $CO_2$ levels reached 419 ppm in 2021—a historic high—and the trend for increasing levels shows little sign of slowing. In response, the search for clean and renewable energy has become one of the greatest challenges for the transition to a more sustainable society.

Electrochemical energy conversion processes driven by renewables, such as wind, hydro, and solar energies, will inevitably be an integral part of any transition away from economies based on fossil fuels [3]. Electrochemical-based renewable energy technologies, such as water splitting and $CO_2$ reduction, will play a key role in the future range of sustainable energy sources and the growing move toward decarbonization of world economies. Electrochemical splitting of water offers a "green" route to generate hydrogen, as opposed to traditional "brown" hydrogen derived from fossil fuels, which involves an energy-intensive gasification process and results in significant $CO_2$ emission. The hydrogen evolved can be used to drive fuel cells—

https://doi.org/10.1016/B978-0-12-822838-8.00006-5

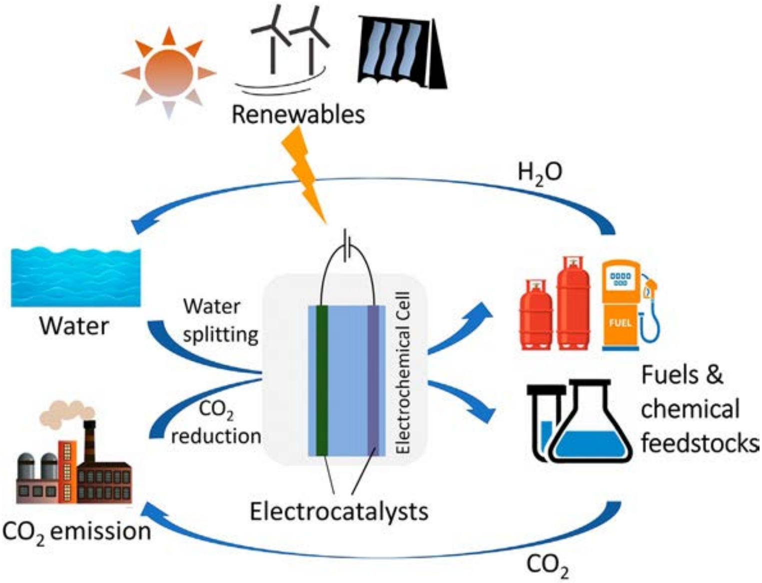

**FIG. 1** The role of Earth-abundant catalysts employed in the electrochemical water splitting and $CO_2$ reduction technologies for sustainable energy production and utilization.

reversing the electrolysis reaction and harnessing the free energy released—providing energy for a myriad of potential transportation and industrial applications without carbon emissions. Similarly, $CO_2$ electrolysis can simultaneously mitigate the elevated levels of this greenhouse gas and can provide a route to valuable carbon feedstocks in place of fossil fuels [4, 5]. The central role of water and $CO_2$ electrolyses, when driven by renewable energy sources, in such approaches is illustrated in Fig. 1.

Widespread implementation of the previously mentioned technologies will require catalysts that will allow these processes to proceed with high yields and at reaction rates that make them economically viable. While some catalysts with the necessary selectivity and rate enhancements exist, they are typically too expensive or rare for large-scale implementation. In contrast, what will be necessary are so-called Earth-abundant catalysts, that is, those that are either carbon-based or composed of relatively common metals, such as iron, nickel, cobalt, or copper, instead of much rarer metals, such as platinum, ruthenium, or gold. The development of Earth-abundant electrocatalysts is therefore critical in any sustainable energy conversion at the scale necessary to address climate change and related issues.

In this chapter, we discuss the syntheses and performance characteristics of scalable Earth-abundant electrocatalysts in the context of sustainable energy conversions, such as electrochemical water splitting and $CO_2$ reduction. Research in this area involves chemical, physical, and theoretical approaches to catalyst performance; these include tuning the electronic structures of catalysts by altering their composition, employing surface engineering techniques such as nanostructuring to optimize interactions with substrates, and computer-assisted catalyst design to inform the synthetic strategies for high-performance electrocatalysts. We also discuss important ongoing challenges of electrochemical conversion technology, particularly catalyst stability. Finally, we address the overall sustainability of electrocatalytic technologies in the context of the life-cycle analysis and end-of-life, emphasizing sustainable approaches to catalyst use, such as the use of recycled materials and renewable resources in catalyst production.

## 2 Fundamentals and principles of electrocatalysis

Electrocatalysts enhance the rate of reactions that occur at electrochemical interfaces, sometimes by many orders of magnitude. As is true for all catalysts, they alter the mechanistic pathways of chemical reactions, lowering the activation energy. While catalysts may be modified to form intermediates during a reaction cycle, these are subsequently transformed in such a way that the original catalyst is regenerated, that is, no net consumption of catalysts occurs. The clean energy innovations described in the introduction will only be realized if suitable catalysts can be engineered to effectively use renewable energy sources to drive key electrochemical processes, such as water splitting and carbon dioxide reduction. We provide in this section a brief overview of the mechanistic details of these important processes.

### 2.1 Mechanism of oxygen and hydrogen evolution reactions

The electrolysis of water involves two half-cell reactions: an oxidation that generates $O_2$, known as oxygen evolution reaction (OER), and a reduction that generates $H_2$, known as hydrogen evolution reaction (HER). Regardless of the pH of the employed media, the overall reaction is described by Eq. (1).

$$2H_2O \rightarrow 2H_2 + O_2 \tag{1}$$

The minimal theoretical voltage to drive the reaction is 1.23 V (vs SHE) under standard conditions. Unfortunately, the reaction is typically very sluggish at this potential, so higher voltages, called overpotentials ($\eta$), are employed to accelerate the rate. The overpotential in an electrolysis is the additional voltage that must be applied to obtain a given current density. Electrocatalysts can significantly lower overpotentials and thereby achieve a given reaction rate at a lower energy input, making the process cheaper to operate. Reaction rates can be measured using either current density or the rate of product generation. The fraction of current associated with the conversion to a particular product is referred to as the Faradaic conversion efficiency (FE). Since OER and HER in water (without electroactive solutes) produces only a single product, FE is usually not reported (but nevertheless recommended when characterizing catalyst performance). For processes that can result in multiple products, such as carbon dioxide reduction, it is much more commonly reported characteristic of catalyst performance.

The mechanisms of the two half-reactions involved in water electrolysis are both multistep processes. OER proceeds via a kinetically slow, multistep transfer process involving four electrons overall. In acidic media, water is oxidized into oxygen and protons (Eq. 2), whereas in the alkaline media, the hydroxide ion is oxidized into water and oxygen (Eq. 3).

$$2H_2O \rightarrow O_2 + 4H^+ + 4e^- \tag{2}$$

$$4OH^- \rightarrow O_2 + 2H_2O + 4e^- \tag{3}$$

The specific mechanism of the oxidation processes involves the generation of hydroxyl radicals, as described later in this chapter. In acidic media, a one-electron oxidation of water results in dissociation and the generation of a hydroxyl radical adsorbed onto the electrode surface, $OH_{ad}$ (Eq. 4); this transient species is then oxidized further to make atomic oxygen (Eq. 5).

$$H_2O \rightarrow OH_{ad} + H^+ + e^- \tag{4}$$

$$OH_{ad} \rightarrow O_{ad} + H^+ + e^- \tag{5}$$

$$2O_{ad} \rightarrow O_2 \tag{6}$$

$$O_{ad} + H_2O \rightarrow OOH_{ad} + H^+ + e^- \tag{7}$$

$$OOH_{ad} \rightarrow O_2 + H^+ + e^- \tag{8}$$

It is generally accepted that molecular oxygen can be generated either through a direct combination of two $O_{ad}$ (Eq. 6) or via an intermediate formed via direct reaction between atomic oxygen and water (Eqs. 7–8) [6]. A similar series of steps, with the same adsorbed intermediates, such as $OH_{ad}$ and $O_{ad}$, proceeds in alkaline media. Specifically, oxidation of hydroxide yields hydroxyl radical adsorbed on the electrode (Eq. 9), followed by $O_{ad}$ formation (Eq. 10), which ultimately generates $O_2$ formation as previously described in acidic media (Eq. 8). Alternatively, $O_2$ is formed via the oxidation of an intermediate formed by reaction of atomic oxygen and hydroxide (Eq. 11).

$$OH^- \rightarrow OH_{ad} + e^- \tag{9}$$

$$OH_{ad} + OH^- \rightarrow O_{ad} + H_2O + e^- \tag{10}$$

$$O_{ad} + OH^- \rightarrow OOH_{ad} + e^- \tag{11}$$

HER is a two-electron process (Eq. 12), the mechanism for which depends on pH. In acidic media, the process is initiated by the reduction of one proton at the electrode, known as the Volmer step (Eq. 13). This is followed by one of two events: either the coupling of two such adsorbed hydrogen radicals, known as the Tafel step (Eq. 14), or the initial reaction between $H_{ad}$ and a proton, followed by a one-electron reduction, the Heyrovsky step (Eq. 15) [6].

$$2H^+ + 2e^- \rightarrow H_2 \tag{12}$$

$$H^+ + e^- \rightarrow H_{ad} \tag{13}$$

$$2H_{ad} \rightarrow H_2 \tag{14}$$

$$H^+ + e^- + H_{ad} \rightarrow H_2 \tag{15}$$

In alkaline media, the net HER (Eq. 16) occurs via a similar reaction pathway as in an acidic solution, except $H_{ad}$ is formed by reduction of water instead of protons. Thus a one-electron reduction of water takes place in the Volmer (Eq. 17) and Heyrovsky (Eq. 18) steps [6]. Energetically, the HER is more difficult in alkaline media owing to the need to break the strong O–H bond in water compared to the weaker O–H bonds of $H_3O^+$; this results in reaction rates that are two to three orders of magnitude lower than in acidic media. The rational design of HER electrocatalysts in alkaline media, therefore, is often centered on the potential for active sites to adsorb and dissociate water and to bind and stabilize key intermediates.

$$2H_2O + 2e^- \rightarrow H_2 + 2OH^- \tag{16}$$

$$H_2O + e^- \rightarrow OH^- + H_{ad} \tag{17}$$

$$H_2O + e^- + H_{ad} \rightarrow OH^- + H_2 \tag{18}$$

## 2.2 Mechanism of $CO_2$ electroreduction

The carbon dioxide reduction reaction (CRR) has inherently large thermodynamic and kinetic barriers owing to the exceptional stability of the substrate. The mechanism of CRR involves three essential elements: chemical adsorption of $CO_2$ on an active site; electron transfer and proton migration steps to cleave C–O bonds and form C–H bonds; and desorption of products from the electrode surface. Depending on the catalyst materials, CRR products can include carbon monoxide, formate, methanol, methane, or ethylene can be formed, as shown in Table 1. Such a variety of products is made possible by the fact that there is a range of possible proton-coupled electron-transfer processes, involving from 2 to 18 electrons (or more). As such, product selectivity is a key challenge in CRR. In contrast to water splitting, for which faradaic efficiency is usually close to 1, the myriad products possible from electrochemical $CO_2$ reduction reaction makes FE a key parameter in characterizing a catalyst's product selectivity. The mechanistic pathway for the formation of several of these products is covered in several excellent review articles [7, 8].

## 3 Types of Earth-abundant electrocatalysts

Highly efficient electrocatalysts typically have high surface areas, good electrical conductivity, and interfacial properties that facilitate interactions with substrates, intermediates, and products. Cost is a key consideration for the widespread large-scale implementation of the technology. For example, oxides of Ru and Ir, both precious metals, are currently benchmark OER electrocatalysts, while Pt is the most efficient HER electrocatalyst [9]. Ag, Au, and Pd, on the other hand, are efficient catalysts for

**TABLE 1** Electrochemical $CO_2$ reduction reactions with equilibrium potentials.

| Number of electrons | Reaction | $E^o$ (V vs SHE) |
|---|---|---|
| $e^-$ | $CO_2 + e^- \rightarrow CO_2^-$ | −1.9 |
| $2e^-$ | $CO_2 + 2H^+ + 2e^- \rightarrow CO + H_2O$ | −0.53 |
| | $CO_2 + 2H^+ + 2e^- \rightarrow HCOOH$ | −0.61 |
| | $2CO_2 + 2H^+ + 2e^- \rightarrow H_2C_2O_4$ | −0.913 |
| $4e^-$ | $CO_2 + 4H^+ + 4e^- \rightarrow HCHO + H_2O$ | −0.48 |
| $6e^-$ | $CO_2 + 6H^+ + 6e^- \rightarrow CH_3OH + H_2O$ | −0.38 |
| $8e^-$ | $CO_2 + 8H^+ + 8e^- \rightarrow CH_4 + 2H_2O$ | −0.24 |
| $12e^-$ | $2CO_2 + 12H^+ + 12e^- \rightarrow C_2H_4 + 4H_2O$ | −0.349 |
| | $2CO_2 + 12H^+ + 12e^- \rightarrow C_2H_5OH + {}_3H_2O$ | −0.329 |
| $14e^-$ | $2CO_2 + 14H^+ + 14e^- \rightarrow C_2H_6 + 4H_2O$ | −0.27 |
| $18e^-$ | $2CO_2 + 18H^+ + 18e^- \rightarrow C_3H_7OH + 4H_2O$ | −0.31 |

$CO_2$ electroreduction to $C_1$-$C_2$ products [10]. The development of Earth-abundant electrocatalysts to replace the efficient but expensive, rare or precious metals is critical if widespread and sustainable use of the technology can be realized (Fig. 2A) [11]. We discuss in this chapter several categories of metallic and metal-free catalysts based on Earth-abundant elements.

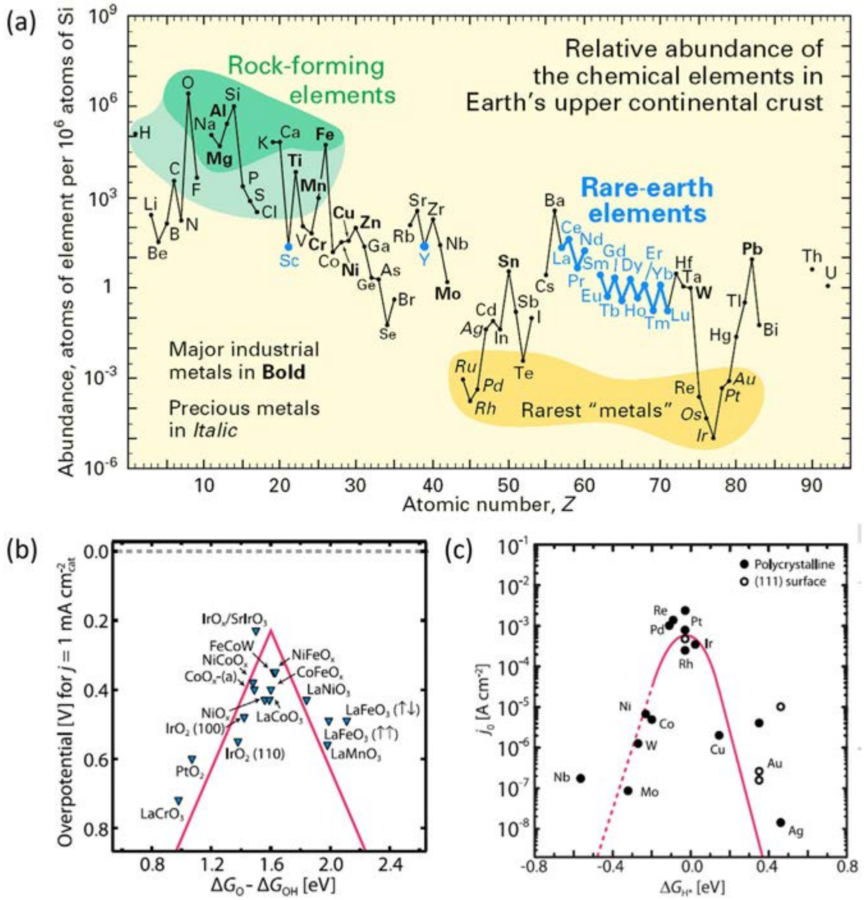

FIG. 2 (A) Relative abundance of the elements in Earth's crust as a function of atomic number. Volcano plots of (B) OER for metal oxides and (C) HER for metals. *Panel (A): Reproduced with permission from G.B. Haxel, J.B. Hedrick, G.J. Orris, Rare earth elements—critical resources for high technology, in: U.S. Geological Survey Fact Sheet 087-02, 2002. Panels (B and C): Reproduced with permission from Z.W. Seh, J. Kibsgaard, C.F. Dickens, I. Chorkendorff, J.K. Nørskov, T.F. Jaramillo, Combining theory and experiment in electrocatalysis: insights into materials design, Science 355 (2017) eaad4998. Copyright © 2017, American Association for the Advancement of Science.*

## 3.1 Metallic catalysts

### *3.1.1 Transition metals, metal oxides, and hydroxides*

Earth-abundant transition metals (TMs), usually defined as those in the first row of the TM block in addition to molybdenum, are widely employed electrocatalysts. Their low cost, their high stability, and the tunability of their properties make TM oxides (TMOs) and hydroxides (TMHs), as well as their pure elemental forms, attractive catalysts for OER, HER, and CRR reactions. The bulk materials of these catalysts, however, are not optimally suited for catalysis: issues such as poor electronic conductivity, low surface area, and limited catalytic-active sites, all hamper catalyst performance. Their catalytic properties can be markedly enhanced with proper physical preparation, such as designing them dimensionally as 0D, 1D, or 2D nanomaterials, or otherwise imparting particular surface morphologies to increase the surface area and the quantity of exposed active sites, all critical factors in improving catalytic performance [12–14].

Oxides and hydroxides of metals, such as Ni, Fe, Co, and Mn, are commonly employed as OER catalysts [15]. As shown in the volcano plot (Fig. 2B), bimetallic oxides such as those composed of Fe/Co, Ni/Fe, and Ni/Co, [16] are among the better OER catalysts, especially under alkaline conditions. In fact, the current state-of-the-art catalyst for OER in alkaline solution using Earth-abundant elements are the bimetallic Ni/Fe TMOs and TMHs. Many studies indicate that loading small quantities of iron to nickel oxide gives rise to significantly enhanced catalytic performance [15, 17]. This is consistent with early work by Corrigan in 1987 that reported an iron loading as low 0.01% in NiO films resulted in significant current enhancement due to OER catalysis [18]. A series of electrochemical, in situ X-ray absorption spectroscopy, and computational work indicates that the superior catalysis of this material is due to the lower overpotential of Fe(III) ions compared to the Ni (III) centers of the bulk oxide [19, 20]. Similarly, ultrathin Ni/Fe double-layered hydroxide have been demonstrated to offer excellent performance in comparison to Ir/C (see Fig. 3A) [21]. A wide range of NiFe-based catalysts deposited on Ni foams and meshes have been investigated [22]. Recently, a new type of Ni-Fe catalyst composed of nanoclusters of γ-FeOOH covalently linked to a γ-NiOOH claimed to have higher OER activity than conventional NiFeOx [23]. A density functional theory computation study suggested the catalyst possessed a bifunctional reaction pathway involving iron as the oxygen-evolving center, and a nearby terrace O site on γ-NiOOH support oxide as a hydrogen acceptor.

TMHs, such as $Ni(OH)_2$ and $Co(OH)_2$, typically exist as two polymorphs, the α- and β-phases. Yan and coworkers synthesized hollow α-$Ni(OH)_2$ spheres, β-$Ni(OH)_2$ hexagonal nanoplates, and β-$Ni(OH)_2$ nanoparticles

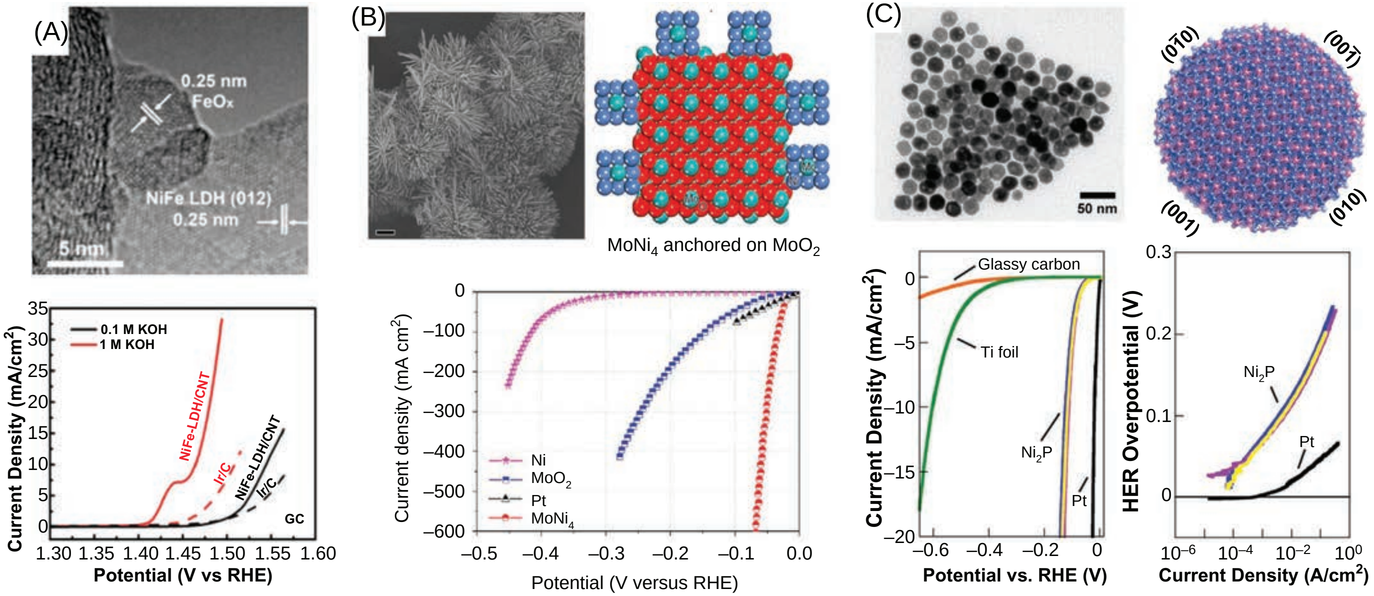

FIG. 3 (A) TEM images of the NiFe-LDH/CNT hybrid and its polarization curve compared to Ir/C in 0.1 and 1.0 M KOH. (B) TEM image of $MoNi_4$, its idealized structural model and polarization data. (C) TEM image of $Ni_2P$ nanoparticles, its structural model, and polarization data. *Panel (A): Reproduced with permission M. Gong, et al., An advanced Ni–Fe layered double hydroxide electrocatalyst for water oxidation, J. Am. Chem. Soc. 135 (2013) 8452–8455, 2013. Copyright © 2013 The American Chemical Society. Panel (B): Reproduced with permission from J. Zhang, et al., Efficient hydrogen production on* $MoNi_4$ *electrocatalysts with fast water dissociation kinetics, Nat. Commun. 8 (2017) 15437. Copyright © Springer Nature 2017. Panel (C): Reproduced with permission from E.J. Popczun, et al., Nanostructured nickel phosphide as an electrocatalyst for the hydrogen evolution reaction, J. Am. Chem. Soc. 135 (2013) 9267–9270. Copyright © 2013 The American Chemical Society.*

via a solvothermal method [24]. Hollow sphere α-$Ni(OH)_2$ was found to have a significantly better OER performance than β-$Ni(OH)_2$, attributed to the presence of highly oxidized Ni species in a γ-NiOOH phase, formed in situ, that facilitates the formation of the OER intermediate species, OOH. Another study reported the synthesis of 2D monometallic cobalt hydroxide microplates by coprecipitation [25]. α-$Co(OH)_2$ was found to exhibit greater OER performance compared to β-$Co(OH)_2$, and the authors suggest the presence of $Co^{2+}$ in the tetrahedral site was more active than $Co^{2+}$ in the octahedral site.

Earth-abundant OER catalysts that are effective in acidic media are rather limited; the benchmark electrocatalysts for these conditions are based on much rarer metals and include materials such as $RuO_2$ and $IrO_2$ [9]. Operation at a neutral pH has been more widely studied, and such mild conditions may offer the advantage of minimizing safety issues associated with the use of caustic or corrosive electrolytes on a large scale. Because manganese oxide is an active center of OER of the oxygen-evolving complex of Photosystem II, initial interest was focused on Mn-based catalysts [26, 27]. It was found that a higher degree of structural disorder for manganese-based catalysts promotes greater catalytic activity. Specifically, OER activity of electrodeposited manganese oxide is enhanced by the presence of coordinatively unsaturated Mn(III) sites, in the form of small manganese-oxo platelets, which readily act as positive holes that effect water oxidation upon the application of an anodic bias [28, 29]. Details regarding the precise oxidation state of the catalyst, however, remain unclear as $MnO_2$ [30], $Mn_2O_3$ [31], or the mixed phase $MnO_x$ [32] have all been reported to catalyze OER activity.

Other Earth-abundant catalysts have been examined in neutral media. One challenge of this work involves the generation of potentially fugitive catalytic species during the course of catalytic pathways, that is, the generation of highly soluble ions as a result of changes in metal oxidation state. Because OER is a four-electron process, the catalyst will necessarily convert between oxidation states during turnover, resulting in some species that are much more substitutionally labile and prone to leaching from the solid catalyst. One solution to this problem was the "self-healing" mechanism reported for cobalt oxide OER catalyst by Nocera and coworkers [33–35]. In this system, Co (II) ions are oxidized and electrodeposited as Co(III) catalytic centers on the electrode surface [34, 35]. During the catalytic cycle, transiently formed Co(II) ions redissolve and leach from the surface, but the inclusion of phosphate in the electrolyte recaptures these ions into the catalyst layer, in effect "healing" the catalyst. Such catalysts have been shown to work effectively in buffered seawater and river water, demonstrating the feasibility of low-cost solar to hydrogen conversion using abundant natural resources [36]. Nickel catalysts with similar self-repairing mechanisms have also been reported in borate-based buffered solutions [37–39].

For HER catalysis, Ni is the most commonly employed TM catalyst in alkaline media because of its high activity relative to other metallic catalysts, such as Mo, Co, and W; this is thought to be due to its low free energy of hydrogen adsorption, $\Delta G_{H*}$, and its high HER exchange current density [40]. Surface morphologies also play a key role in HER activity for nickel catalysts. In one example, nickel dendrites, which have large surface areas with highly (111)-populated facets at the sharp edge, contribute to high HER activity [41]. Carbon support materials, such as graphene and carbon black, are often employed to ensure high and homogeneous dispersion of active sites. Single-atom nickel doped on nanoporous graphene, for example, exhibits highly efficient and stable HER; *sp-d* charge transfer between the Ni dopants and the carbon atoms [42] is thought to play a key role in enhancing catalytic efficiency in this case. In addition, $MoNi_4$ (Fig. 3B) exhibits an overpotential of 15 mV at 10 mA cm$^{-2}$ in 1 M KOH [43]; fast water dissociation kinetics has been invoked to explain its catalytic performance.

There are several examples of HER catalysts other than nickel that are also noteworthy. Cobalt embedded on nitrogen-rich carbon nanotubes (CNTs) exhibits high activity and stability at all pH ranges; a synergetic relationship between the nitrogen dopants and carbon-coated Co nanoparticles (NPs) is thought to play a crucial role in the observed catalytic performance [44]. Ultrathin nanosheets of $MoO_2$ on nickel foam has excellent HER characteristics relative to compact $MoO_2$ [45] owing to a high surface area and a greater number of exposed active sites. Likewise, nanostructures of $MnO_2$ [46] and $WO_2$ [47, 48] have abundant oxygen vacancies and active sites that promote conductivity and favorable $H^+$ adsorption. Finally, of increasing interest is research on bifunctional catalysts for overall water splitting; this approach may simplify catalyst development and incorporation in electrochemical cells [44, 45]. Examples include bimetallic catalysts, such as $NiCo_2O_4$ [49], $NiFe_2O_4$ [50], and $NiFeO_x$ [51].

A wide range of metals have served as catalysts for $CO_2$ electroreduction, including Co, Zn, and Cu; products such as formate ($HCOO^-$), carbon monoxide (CO), and even more highly reduced products such as hydrocarbons and alcohols [52, 53] have been reported. Xie and coworkers reported $CO_2$ reduction using 2D nanosheets of $Co_3O_4$; these have a high fraction of low-coordinated surface atoms that serve as active sites and enhance $CO_2$ adsorption and also have high electronic conductivity that enhances the reduction of $CO_2$ to formate [54]. Sheet thickness of this catalyst strongly influences catalytic activity; 1.72 nm thick $Co_3O_4$ ($FE_{HCOO-} = 64\%$) was found to have ~1.5 and 20 times greater performance relative to 3.51 nm thick sheets and the bulk material, respectively. In further studies, enhanced intrinsic activity and higher formate selectivity ($FE^{-}_{HCOO} = \sim 90\%$) was observed in a 4-atom-thick partially oxidized Co atomic layer than the corresponding 4-atom-thick samples of pure Co [55].

Oxide-derived Zn prepared by the lithium electrochemical tuning method, which entails reduction of the oxide precursors and results in grain boundaries that are enriched in catalytic-active sites, reduces $CO_2$ to CO with $FE_{co}$ of ~91% [56]. In another study, porous Zn obtained by the electrodeposition on a Cu mesh substrate had a reported $FE_{co}$ of over 95% [57].

Cu is an excellent CRR catalyst and the only pure metal that reduces $CO_2$ to products such as hydrocarbons, aldehydes, and alcohols, all of which involve net reductions of more than two electrons. Surface preparation of copper CRR catalysts has been shown to be critical. Hori et al. reported the first oxide-derived Cu catalyst; a porous catalyst with a very high surface area was yielded upon reduction of the copper oxide [58]. Kanan and coworkers reported the preparation of an active catalyst, with grain boundaries rich in surface terminations, via thermal oxidation of Cu foils in air and subsequent electroreduction of the $Cu_2O$ [59]. Other surface oxidation approaches, such as oxygen plasma [60], chemical growth [61], and electrochemical deposition [62], have been successfully used in the preparation of electrocatalysts for $CO_2$ conversion to $C_{2+}$ products. It should be noted that both the choice of electrolyte and cell design (e.g., laboratory H-cell vs flow cell) have significant impacts on the current densities and product selectivity [63]. In a striking demonstration, Sargent and coworkers obtained ~70% selectivity in $CO_2$ conversion to ethylene at −0.55 V vs RHE for 150 h in 7 M KOH based on a gas-phase $CO_2$ electrolyte flow system [64]. They found that the highly alkaline electrolyte significantly decreased the ohmic overpotentials but required the use of a flow cell, as opposed to an H-cell, as KOH readily reacts with $CO_2$ to form bicarbonate salts.

### *3.1.2 Transition metal dichalcogenides*

TM dichalcogenides (TMDs), which have the general formula $MX_2$ (where M is the TM and X is usually sulfide, S, or selenide, Se), are semiconducting materials that possess intriguing structural and electronic properties and represent an attractive class of electrocatalysts for HER and CRR processes. The preparation of TMDs as catalysts typically involves engineering to fabricate 2D materials because the bulk compounds usually exhibit poor catalytic properties.

Hinnemann et al. published density functional theory calculations in 2005, which suggested the free energy change associated with atomic hydrogen bonding to the Mo (1010) edge site of $MoS_2$ was close to zero, suggesting its suitability as a HER catalyst [65]. This was followed by the experimental confirmation that the number of edge sites of $MoS_2$, as measured by scanning tunneling microscopy, is proportional to HER activity [66]. This finding led to the optimization of $MoS_2$ as a HER electrocatalyst by enhancing the edge to basal plane ratio [67]. A variety of related strategies for further enhancement of catalytic properties were also reported for TMD catalysts. These included: the introduction of defects to the basal plane of $MoS_2$ [68, 69]; interface and strain engineering through hybridization with support structures [70, 71]; and phase engineering to change the TMD bandgaps, which enhances charge-transfer kinetics [72, 73].

$MoSe_2$ catalysts have not be as extensively studied as the sulfide analog, but excellent HER results have been reported from $MoSe_2$ nanosheets [74] and heterostructures consisting of single- or few-layer $MoSe_2$ flakes and carbon nanomaterials [75]. Similar strategies for developing HER catalysts have been reported for W [76], Co [77], Fe [67], and Ni [78]. Zhang and coworkers reported a simple hydrothermal treatment using iron foam with thiourea to form FeS nanosheets that, upon electrochemical activation, formed $Fe@FeO_xS_y$, which performs well for both HER and OER [79]. TMDs such as $MoS_2$ [80] and $WSe_2$ [81] have been employed for $CO_2$ electroreduction to CO in ionic liquid electrolytes. Attributed to the low work function and strong binding energies toward $CO_2$ reduction intermediates, $WSe_2$ nanoflakes show overpotentials as low as 54 mV. Doping of $MoS_2$ with 5% niobium resulted in enhanced conversion to CO [82] due to changes in the binding energies of intermediates to $MoS_2$ edge atoms.

TMD use as electrocatalysts for OER has not been as widely investigated. Amorphous- Ni-Fe-S ultrathin nanosheets exhibit a porous 3D architecture that promotes efficient charge and mass transport, resulting in a high OER performance [83]. In another example, the challenge of insufficient active sites in bulk $CoSe_2$ was overcome by exfoliating the $CoSe_2$-based inorganic–organic lamellar nanohybrids to atomic thicknesses [84]. This ultrathin $CoSe_2$ was found to contain a large number of vacancies that serve as active sites to efficiently catalyze OER.

### *3.1.3 Other metal-based materials*

TM phosphides (TMPs) are an interesting class of materials showing excellent catalytic activity and stability, mainly for HER reactions [85]. TMPs can be viewed as the doping of P atoms into the crystal lattices of TMs. The electronegative P atoms draw electrons from metal atoms, enhancing their basicity and ability to trap protons. For example, $Ni_2P$, is an outstanding Earth-abundant HER catalyst in acidic media. This is consistent with the theoretical prediction that phosphorus leads to moderate bonding of relevant intermediates and products on the catalyst surface [86]. In 1995, Paseka et al. reported the high HER activity of amorphous $NiP_x$ with a low content of phosphorus (~3 wt%) [87].

Based on similarities between hydrodesulfurization (HDS) and HER, Popczun et al. investigated $Ni_2P$ (001), a well-known HDS catalyst, and found that nanoparticles of this material are highly effective HER catalysts (Fig. 3C) [88]. Phosphides of other metals such as Co [89], Fe [90], and Mo [91] have also been shown to have excellent HER performance.

A wide range of TM nitrides (TMNs) and carbides (TMCs) can be formed by embedding nitrogen or carbon atoms into the interstices of parent metals. The intercalation of nitrogen or carbon atoms broadens the d-band of the metal and redistributes the density of states near the Fermi level [92]. The presence of nonmetal elements in the metal lattice allows the alteration of the TMN's electronic structure to resemble those of noble metal-based catalysts such as Pt [93]. Mo- and W-based TMNs/TMCs are the two most commonly investigated that show remarkable HER activities and excellent corrosion resistance and stability.

Metal–organic frameworks (MOFs), a rapidly growing class of porous materials that consist of networks of metal ions or clusters coordinated to organic ligands, have been extensively explored as electrocatalysts [94]. The possible range of metal-ligand junctions in MOFs permits the fabrication of heterostructures with highly tunable electronic and chemical properties. Zhao et al. reported an ultrathin NiCo MOF for efficient OER in alkaline media; electronic coupling of coordinatively unsaturated Ni and Co ions in active centers is implicated in catalyst performance [95]. NiFe-based MOFs grown on a flexible 3D macroscopic nickel foam exhibit superior OER performance and can also catalyze HER, making them promising candidates for bifunctional catalysts that can effect overall water splitting [96]. Kornienko et al. synthesized thin films of atomically defined and nanoscopic cobalt porphyrin MOFs that catalyze the reduction of $CO_2$ to CO in aqueous electrolytes [97].

Earth-abundant p-block elements, such as Sn and Bi, are known to be active catalysts for the electroreduction of $CO_2$ to formate. The high formate activity observed with Sn was proposed to originate from an optimal binding energy toward *OCHO, a key intermediate in the process [98]. A strong size dependence of $SnO_2$ particles was observed: particles of ~5 nm were found to exhibit the highest $FE_{HCOO^-}$ (~ 93%) with an overpotential of ~340 mV [99]. This is consistent with another study on grain boundary-rich, ultra-small interconnected $SnO_2$ nanoparticles with sizes <5 nm; this material promoted formate production by suppressing $H_2$ generation [100]. Similarly, nanostructuring of bulk Bi to morphologies, such as nanoparticles [101], dendrites [102], and nanoflakes [103], enhances CRR catalysis. Bimetallic systems such as Cu/Sn [104] and Bi–Sn [105] were also found to promote CRR.

## 3.2 Metal-free nanomaterials

The discovery of nitrogen-doped CNTs as a metal-free catalyst for oxygen reduction reaction by Dai and coworkers in 2009 initiated the development of a range of metal-free catalysts [106]. Metal-free catalysts based on abundance resources of carbon materials offer a low-cost alternative to metallic catalysts and may possess advantages in terms of long-term stability.

### *3.2.1 Graphene*

The discovery of graphene by Geim and Novoselov in 2004 initiated widespread investigation of this 2D material for various potential applications [107]. Graphene's large specific surface area, good electrical conductivity, and tunability of its electronic and surface properties, make it an attractive candidate for electrocatalytic applications. As discussed earlier, graphene is an excellent support material for anchoring single-atom catalysts. As a 2D material, the edge of graphene is found to be significantly more active for electrocatalysis than the basal plane [108]. Consequently, engineering of 3D graphene networks to produce abundance sharp edge sites is found to promote the adsorption and reduction of protons, resulting in enhanced HER catalysis [109].

An effective approach to enhancing the electrocatalytic performance of graphene is by heteroatom doping with, for example, nitrogen, sulfur, and boron. Moreover, dual-doped graphene have shown even higher electrocatalytic HER activity than singled-doped analogs. In one example, graphene doped with both nitrogen and phosphorus showed enhanced HER catalytic activity that was ascribed to coactivation of adjacent carbon atoms via modulation of valence orbital energy levels [109]. Similarly, Chen and coworkers reported that codoping of N and S on nanoporous graphene resulted in HER kinetics comparable to $MoS_2$; the researchers attributed this to a synergetic effect from both dopants at lattice defects, resulting in rapid electron transfer [110]. Qiao and coworkers evaluated the HER performance of a series of codopant combinations based on N-doped graphene, with the second dopant being phosphorus, silicon, or boron [111]. It was found that the N/S codoped graphene was the most active HER catalyst in the series; this material possessed a Fermi level value of 0.23 eV, significantly smaller than the 0.81 eV exhibited by singly doped N-graphene (Fig. 4A). The decrease of the Fermi level enhances $H_2$ adsorption and, consequently, HER performance.

The impact of graphene heteroatom doping is also profound for CRR, especially N-doping. Wu et al. doped graphene with nitrogen at various levels via chemical vapor deposition and found the highest nitrogen level

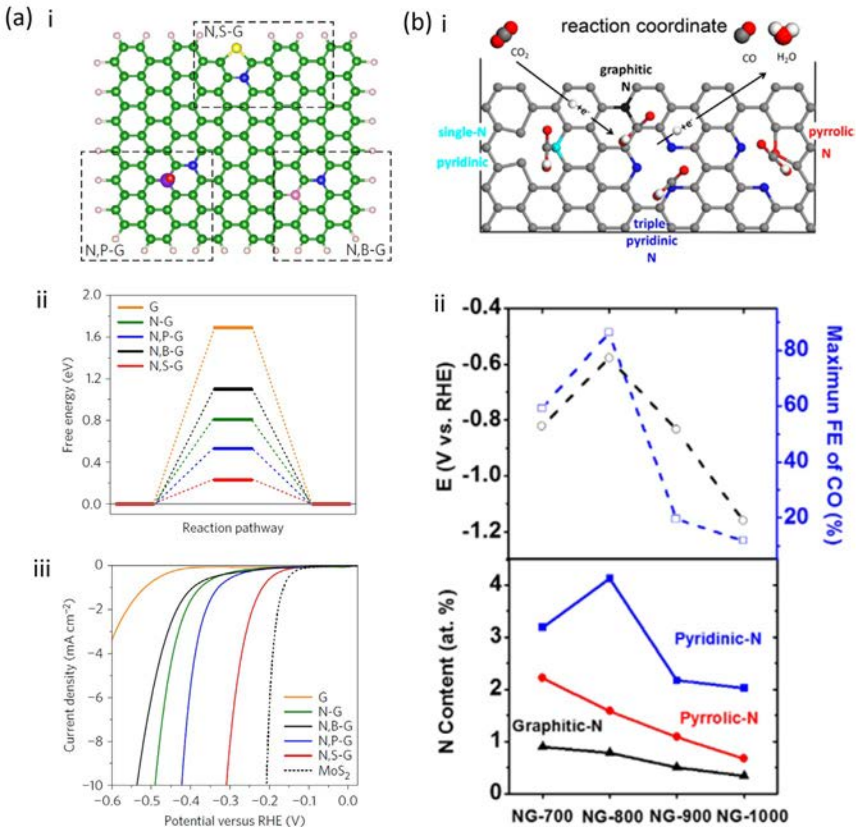

**FIG. 4** (A) Dual-doped graphene models with (i) atomic configurations and (ii) Fermi level energies; (iii) current density data with N, B, P and S dopants. (B) (i) Structure of N-doped graphene and its $CO_2$ reduction pathway, and (ii) maximum Faradaic efficiency of CO and its corresponding potential versus nitrogen functionality. *Panel (A): Reproduced with permission from Y. Jiao, Y. Zheng, K. Davey, and S.-Z. Qiao, Activity origin and catalyst design principles for electrocatalytic hydrogen evolution on heteroatom-doped graphene, Nat. Energy 1 (2016) 16130. Copyright © Springer Nature 2016. Panel (B): Reproduced with permission from J. Wu, et al., Incorporation of nitrogen defects for efficient reduction of CO2 via two-Electron pathway on three-dimensional graphene foam, Nano Lett. 16 (2016) 466–470. Copyright © 2016 The American Chemical Society.*

catalyzes the electroreduction of $CO_2$ to CO with an $\text{FE}_{\text{co}}$ of ~85%; pyridinic nitrogen atoms in the graphene matrix serve as the most active catalytic sites [112] (Fig. 4B). This result is consistent with other systems, such as N-doped CNTs, where it was proposed pyridinic defects retain a lone pair of electrons that enhance $CO_2$-binding [113]. Wang et al. found melamine as a pyridinic precursor for N-doped graphene achieved $\text{FE}_{\text{HCOO-}}$ conversion of 73%, whereas thiourea, polypyrrole, polyaniline, and dicyandiamide as precursors exhibit either no or minimum activity toward CRR [114].

### *3.2.2 Graphitic carbon nitride*

Graphitic carbon nitride ($\gamma$-$C_3N_4$) is a polymeric semiconductor with a bandgap of ~2.7 eV that has been shown to be an effective photocatalyst [115, 116]. Its unique electronic structure, high nitrogen content (theoretically up to 60%), and excellent chemical stability suggest that it could also serve as an electrocatalyst. The nitrogen-rich carbon framework is an important feature that can enhance interactions with substrate molecules as discussed previously in the context of N-doped graphene. Experimental and theoretical studies indicate pyridine-like nitrogen centers, in a triazine-like configuration, is likely related to the electrocatalytic active sites [117].

Despite the advantages of the $\gamma$-$C_3N_4$ structure, the limited surface area and poor conductivity are challenges that need to be overcome to realize satisfactory catalytic performance of this material. Bulk $\gamma$-$C_3N_4$ is relatively catalytically inert but 2D-engineered materials have greater surface areas and possess more structural defects and surface termination sites, all of which can enhance catalytic activity. Thin 2D nanostructures also enhance electron mobility, shortening the electron-transfer pathway to the active nitrogen sites. Incorporation of $\gamma$-$C_3N_4$ onto other conductive materials can also improve electrocatalysis. In one example, the coupling of $\gamma$-$C_3N_4$ with nitrogen-doped graphene showed an unexpectedly high HER activity, with a comparable overpotential and Tafel slope to metallic catalysts [118]. It was proposed that the observed electrocatalytic properties originate from chemical and electronic coupling that promote proton adsorption and reduction kinetics.

The abundance of pyridinic-N sites in the $\gamma$-$C_3N_4$ framework results in a strong affinity for $CO_2$ and strong adsorption of oxygen-bound intermediates on carbon sites, thereby facilitating CRR [119]. Lu et al. proposed that the enhanced electrocatalytic activity of $\gamma$-$C_3N_4$/multiwall carbon nanotubes (MWCNTs) toward $CO_2$, which had an $FE_{co}$ of 60%, is attributable to the formation of active carbon–nitrogen bonds, high specific surface area, and improved conductivity of the composite material [120]. Evidence of the importance of such hybrid structures is reflected by the fact that neither pure $\gamma$-$C_3N_4$ nor undoped MWCNTs exhibit significant CRR activity. $\gamma$-$C_3N_4$ can also serve as an excellent platform as a molecular scaffold for TM coordination. For example, Jiao et al. prepared a Cu-$\gamma$-$C_3N_4$ complex that showed intramolecular synergetic catalysis capable of generating $C_2$ species, such as ethanol and ethylene [119].

## 4 Catalyst preparations and strategies in enhancing electrocatalytic performance

The previous section describes a range of high performance and promising OER, HER, and CRR electrocatalysts based on inexpensive, Earth-abundant elements. The success of any such electrocatalyst will ultimately rely on synthetic strategies aimed to modify the structural properties of the catalysts to enhance surface morphologies, optimize thicknesses, and promote defect formation, all of which can significantly enhance electrocatalytic performance. In this section we discuss several common low-cost catalyst synthetic approaches to improve catalyst performance (Fig. 5) and catalyst design strategies (Fig. 6).

## 4.1 Common methods of catalyst preparation

### *4.1.1 Hydrothermal synthesis, impregnation, and coprecipitation*

Hydrothermal, impregnation, and coprecipitation are commonly employed approaches for the syntheses of a wide range of electrocatalysts. These low-cost, wet chemical methods allow for the formation of tailor-made, ultrafine, homogeneous, and high purity electrocatalysts. The simplicity and flexibility in controlling the composition and morphology of the material is achievable by varying the precursors, including metal salts and nonmetal sources, and reaction conditions, such as temperature, concentration, duration, and pH. In addition, the hydrothermal approach allows for one-pot synthesis of electrocatalysts by directly forming nano-dimensional catalysts on conductive support materials. For example, Gao et al. successfully prepared via this method a Cu/Co/W mixed metal oxide on copper foam that was demonstrated to be an efficient and stable electrochemical water-splitting catalyst [121]. The advantage of hydrothermal preparative methods is illustrated by Fig. 5A, which depicts the rational composition of mixed catalyst systems. In this example, cobalt oxides serve as high-performance OER and HER catalysts, semiconducting copper oxides enhance electron transport, and tungsten oxides offer structural and chemical stability. To prepare atomically dispersed metal catalysts, distribution of a metal precursor on the support is typically achieved via wet impregnation, coprecipitation, or deposition–precipitation [122]; extremely low concentrations of metal precursors are usually employed, resulting in relatively homogenous metal loading on the support substrates.

### *4.1.2 Electrochemical methods*

In electrodeposition techniques, catalysts are precipitated on conductive substrates via the application of an external direct or pulsed current. A wide range of nanostructured materials, such as metal nanoparticles, nanowires, nanosheets, and 3D-hierarchical structures, can be directly formed on conductive substrates [123]. To obtain high current densities, electrodeposition is typically performed on high surface area substrates, such as nickel meshes, nickel foams, and carbon papers [124–126]. Significantly, those support structures are important for catalyst functionality as

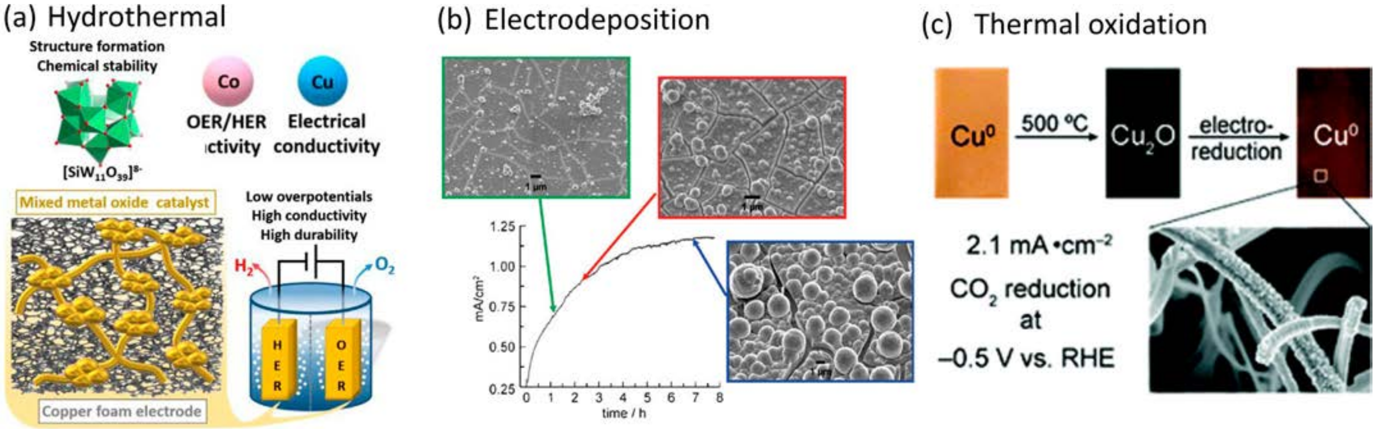

**FIG. 5** Examples of electrocatalyst preparative methods. (A) A rational mixture of metallic elements in the hydrothermal synthesis of Cu/Co/W mixed metal oxide on a copper foam as a bifunctional OER and HER catalyst. (B) In situ electrodeposition of Co/$P_i$ OER catalyst, with the SEM images obtained at indicated times during the electrodeposition. (C) Thermal oxidation of Cu to form $Cu_2O$, which is subsequently reduced to form a porous Cu CRR catalyst. *Panel (A): Reproduced with permission from D. Gao, R. Liu, J. Biskupek, U. Kaiser, Y.-F. Song, C. Streb, Modular design of noble-metal-free mixed metal oxide electrocatalysts for complete water splitting, Angew. Chem. Int. Ed. 58 (2019) 4644–4648. Copyright © 2019 The Royal Society of Chemistry. Panel (B): Reproduced with permission from M.W. Kanan, Y. Surendranath, and D.G. Nocera, Cobalt–phosphate oxygen-evolving compound, Chem. Soc. Rev. 38 (2009) 109–114. Copyright © 2009 The Royal Society of Chemistry. Panel (C): Reproduced with permission from C.W. Li, M.W. Kanan,* $CO_2$ *reduction at low Overpotential on cu electrodes resulting from the reduction of thick* $Cu_2O$ *films, J. Am. Chem. Soc. 134 (2012) 7231–7234, 2012. Copyright © 2012 The American Chemical Society.*

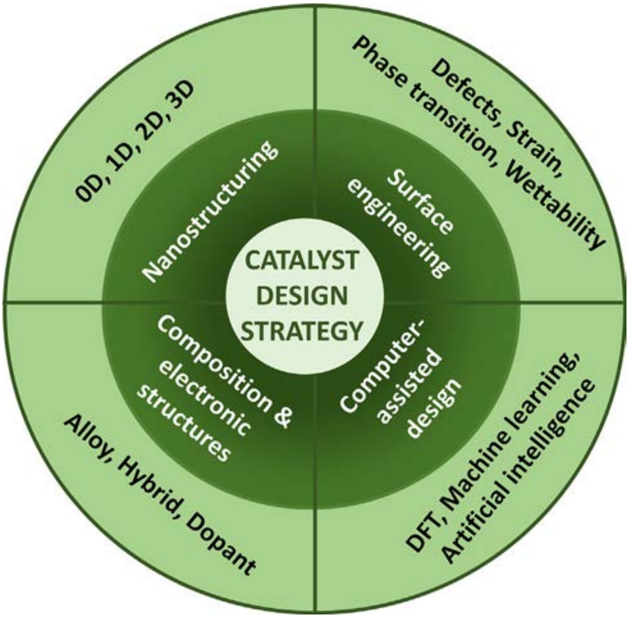

**FIG. 6** Scheme of the common strategies employed in the electrocatalyst design.

they also facilitate reactant and product mass transport. In situ electrochemical deposition was used to prepare the previously mentioned self-healing Co-$P_i$ OER catalyst (Fig. 5B) [33, 34, 127]. Anodization is another electrochemical approach and offers a strategy to form thick, high surface area structures [128]. In one example, anodization of polycrystalline Cu foil in concentrated KOH formed $Cu(OH)_2$ nanowires, which, upon reduction, formed a Cu catalyst with mixed oxidation states that favored ethylene production [129, 130].

### *4.1.3 Others*

The preparation of catalysts by doping either metals or heteroatoms on conductive supports often requires a calcination step to ensure strong physical bonding and to prevent particle agglomeration [122]. This step decomposes the impregnated metal salts, such as nitrates, chlorides, carbonates, and organic chelates, leaving a metal or metal oxide on the support surface. Calcination is also an important step used to enhance the crystallinity of materials. The properties of catalysts are significantly affected by the temperature and heat-treatment atmosphere employed during calcination. Thermal oxidation also offers an effective way to fabricate a large surface area and porous catalyst by initially forming an oxide layer, which can be reduced to a metallic state that is active for CRR (Fig. 4C) [59].

One of the more scalable methods in the production of 2D materials is ultrasonication, which can be employed as a standalone or a complimentary processing technique [131]. In addition, bimetallic alloys, core-shell structures, and supported nanoparticles can be synthesized via sonoelectrochemistry [132]. To form porous structures, the use of templates and dealloying methods has been reported. For example, Li et al. prepared a bifunctional electrocatalyst for overall water splitting by coating $NiCo_2S_4$ nanotubes with a nitrogen-doped carbon layer via the use of polyacrylonitrite (PAN) as a template [133]. Wang et al. reported the preparation of nanoporous and amorphous Ni-Fe-P array on Ni foam via electroless plating of component ionic precursors followed by fast dealloying in 1.5M HCl [134].

Chemical vapor deposition (CVD) is an ideal method for forming thin metal films. CVD involves incorporation of heteroatoms during the growth process by mixing in a N-containing reagent [135]. This method allows the graphene material to retain many of the intrinsic physical and chemical properties of the pure material and provides new catalytic properties. Single or metal alloys can be fabricated by CVD using either monometallic or heterometallic precursors, respectively [136].

## 4.2 Catalysts design strategies

### *4.2.1 Nanostructuring*

It is well established that the activity and selectivity of a given electrocatalyst are determined by the number of active sites and their intrinsic activity [137]. Relative to bulk materials, reducing particle sizes typically enhances catalyst performance by increasing the number of catalytically active sites and by exposing much larger surface areas. Furthermore, nanoscale morphology can be engineered to modulate electrocatalytic activity and selectivity. Thus, a number of the highly efficient electrocatalysts described earlier in this chapter are in the form of nanoscale materials. One-dimensional nanostructures, such as nanorods, nanofibers, and nanowires, have extensive exposure of specific facets due to preferential crystal growth; this structure greatly enhances electron transport properties that may be advantageous for highly efficient electrocatalysis [138]. For example, 1D $NiCo_2P_x$ nanoneedles on carbon felt have HER activity comparable to commercial Pt/C catalysts [139]. Several examples of catalysts composed of various 2D nanomaterials in the form of nanosheets, nanoplatelets, and more were described in detail earlier in this chapter.

### *4.2.2 Tuning catalyst composition and electronic structures*

Modifying a given catalyst's composition, via atomic substitution, for example, will change its electronic structure. Diaz-Morales and coworkers systematically demonstrated that superior electrocatalytic activity can be achieved by rational doping [140]. They found that when the atomic nickel sites are partially replaced by iron, manganese, or chromium, the OER overpotential can be markedly reduced. They attribute this to enhanced compatibility between the electronic structures and binding strengths between the OER intermediates and the electrocatalyst surfaces. Mixed metallic catalysts typically show more promising performance than those based on single metals. Similarly, the integration of two or more different materials that are intimately bonded in heterostructures may result in synergetic effects at the material interfaces, improving electrocatalytic activity. For example, in $Ni(OH)_2/MoS_2$, hetero-interfaces reduce the energy barrier of initial water dissociation and the subsequent $H_2$ generation [141]; in this case, $Ni(OH)_2$ provides the active sites for –OH adsorption, while $MoS_2$ enhances the adsorption of H* intermediates.

Metal-based catalysis generally involves d-bands with energies close to the Fermi level. Alloying is one of the most efficient way to engineer the d-band vacancy of a metal-based catalyst to control catalytic performance. For example, neither Cu nor Ti are good HER catalysts, however, the use of CuTi alloy with optimal electronic structure and hydrogen binding energy results in a high HER performance [142]. Similarly the use of $MoNi_4$ alloy (Fig. 3B), with significantly improved electronic structure and outstanding water dissociation ability, enhances HER activity in an alkaline medium [43]. Heteroatom doping on graphene [110, 111], as detailed earlier, is another effective strategy used to alter the electronic properties of the catalysts that leads to enhanced electrocatalytic performance.

Vacancy engineering of an electrocatalyst can effectively modulate the local atomic structure, thereby creating local low-coordinate geometries and concomitant changes electron configurations. For example, Sun et al. demonstrated that ultrathin $Co_3O_4$ offers a considerably large fraction of coordinatively unsaturated surface atoms that serve as active sites to facilitate the OER [143]. Oxygen vacancy-engineered catalysts could also overcome the low electrical conductivity issue of TMOs. Wang et al. reported that reduced mesoporous $Co_3O_4$ nanowires with abundant oxygen vacancies have lower charge-transfer resistance than the pristine $Co_3O_4$ nanowires [144].

### *4.2.3 Interfacial engineering*

Since electrocatalysis proceeds primarily on the surfaces of catalysts, rational design of the exposed surface to include different coordination environments can affect the adsorption sites as well as the binding strengths of reactants and reactive intermediates. As such, surface engineering makes possible significant improvements of catalyst performance for a given material. Many catalysts have specific facet-exposed sites that exhibit high catalytic activity; for example, $Co_3O_4$ nanocrystals exposed with {111} facets display enhanced charge-transfer characteristics and correspondingly improved HER and OER performance [145]. Introducing surface defects can profoundly influence the electron configurations and, consequently, the chemical processes at the surfaces of the catalysts. Zhao et al. demonstrated that the metal or oxygen vacancies can endow NiFe-LDH nanosheets (where LDH = layered double hydroxide) with semimetallic conductivity, enhancing charge-transfer kinetics and improved OER activity [146]. Furthermore, combining crystal strain effect to the defect engineering, Li et al. reported the greatly improved HER activity of $MoS_2$ through the formation of strained sulfur vacancies [147]. Phase transitions provide yet another surface engineering strategy. For example, a transition from the semiconducting 2H phase to the metallic 1T phase of $MoS_2$ via Li ion intercalation was found to significantly improve the conductivity and charge-transfer kinetics, enhancing overall HER performance as a result [148].

### 4.2.4 *Computer-assisted catalyst design*

The use of computation modeling has greatly contributed to progress in catalyst development in recent years. Density functional theory (DFT) can provide insights on the electronic structure of catalytic materials in their own right but also on adsorption energy and other variables relevant to catalyst activity, selectivity, and stability [149]. DFT has been employed to explain experimental phenomena, predict experimental results, and guide catalyst design. DFT calculations are usually supported by data from analytical techniques, such as high resolution transmission electron microscopy, spectroscopic, and electrochemical measurements. For example, to examine the origin of electrocatalytic activity of nonmetallic heteroatom-doped graphene, Jiao et al. correlated the relationship between DFT calculations and data from structural characterization techniques and electrochemical experiments [111]; they constructed volcano plots to demonstrate the inherent activity trends for different dopants (e.g., B-, N-, O-, S-, P-doped) on graphene samples and predicted electrocatalytic properties that were consistent with experimental results. Tran and Ulissi recently reported an artificial intelligence approach, combining machine learning and optimization to guide DFT calculations and to develop a fully automated screening method [150]. They screened alloys of 31 different elements and identified 131 candidate surfaces across 54 alloys for CRR, and 258 surfaces across 102 alloys for HER, for experimental validation.

# 5 Durability challenges of electrocatalysts

The durability of a catalyst refers to its ability to operate and retain high activity over an extended period. It is a critical factor in the economic viability of any large-scale process based on renewable energy, having a substantial impact on the operational and maintenance costs of electrolyzers. Despite the many recent developments in the area of catalysts based on earth-abundant elements, their durability remains a significant challenge. We discuss here the characterization protocols of durability testing (Fig. 7A), factors that lead to catalyst degradation (Fig. 7B), and the mitigation strategies to enhance catalyst durability.

## 5.1 Durability testing and characterization

Durability studies of electrocatalysts are usually done via galvanostatic (applying current) or potentiostatic (applying voltage) methods under optimal experimental conditions. In the former, catalyst performance is measured relative to a given current density, usually at least 10 mA cm$^{-2}$, and for durations ranging from a few to several hundred hours; in the two-electrode full-cell system, the measurement of cell potential difference offers information on energy efficiency. In potentiometric methods, which are suitable for the OER and HER, the overpotential before and after a multiple potential cycling (e.g., 10,000 runs) is measured by cyclic voltammetry (CV) or linear sweep voltammetry (LSV); the change in magnitude of the overpotential defines the durability of the electrocatalysis. In addition, accelerated durability test protocols are sometimes employed to elucidate catalyst degradation mechanisms and examine the stability of other relevant electrolyzer components, such as membranes [151, 152].

Prior to durability testing, the surface morphology and chemical composition of the catalyst layers are usually characterized using standard techniques, such as scanning electron microscopy, transmission electron microscopy, X-ray diffraction, X-ray photoelectron spectroscopy, and Raman spectroscopy. In addition, electrochemical techniques, such as CV, LSV, and electrochemical impedance spectroscopy, are used to characterize electrocatalytic properties, such as onset potential, electrochemical active surface area, and resistivity information. After a long-term experiment, the previously named characteristics are reexamined to quantify changes in the intrinsic catalytic activity that could result from catalyst degradation, such as agglomeration, poisoning, or a reduction in active surface area. Changes in surface morphology can provide insights on the structural integrity and stability of the catalyst. Similarly, changes in chemical composition could indicate the presence of adsorbed species or catalyst poisoning.

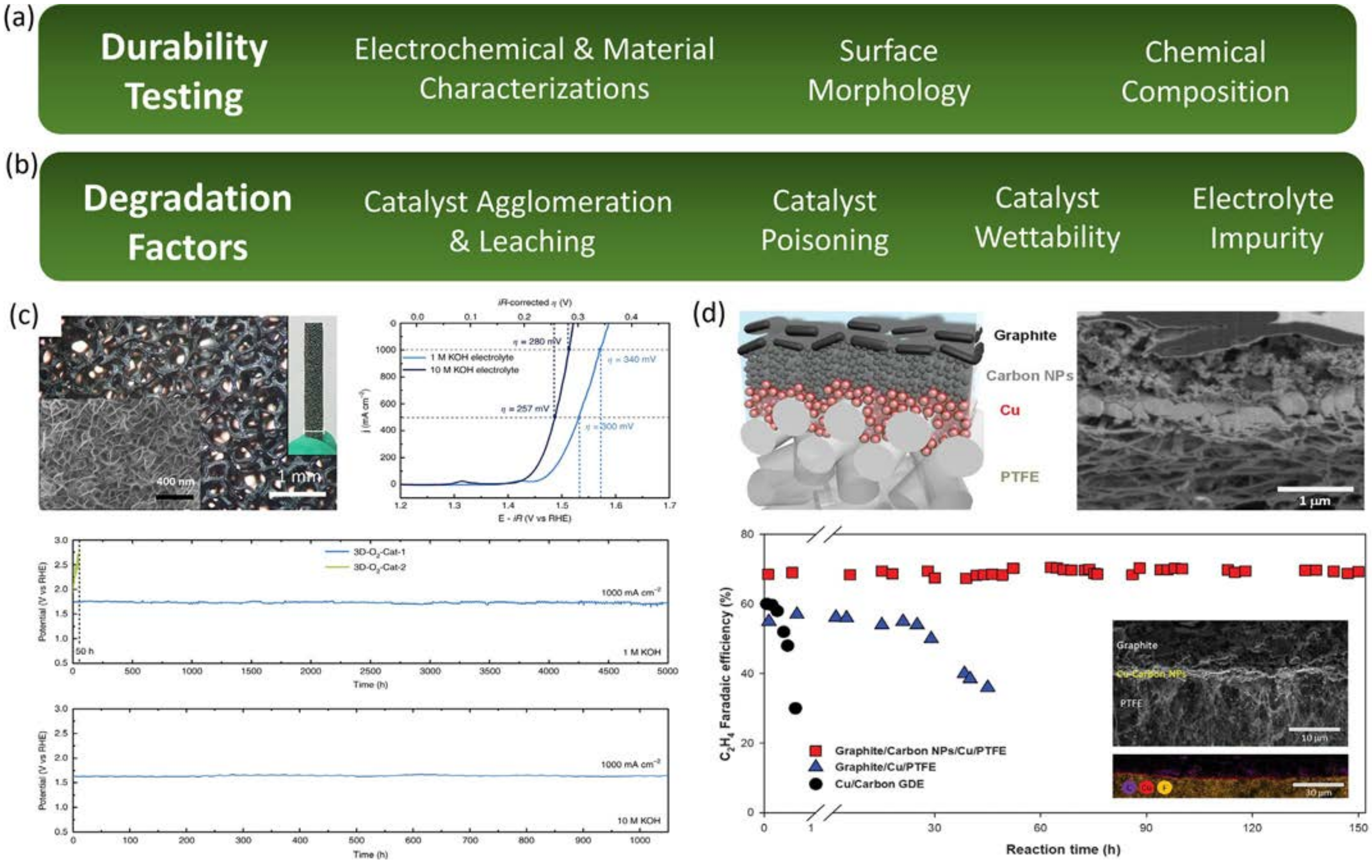

**FIG. 7** Lists of parameters for (A) catalyst durability testing and (B) factors that cause degradation. (C) Optical and SEM images of layered double hydroxides nanosheets derived from iron corrosion engineering strategy. Polarization curves at large current densities in 1 and 10 M KOH. Long-term stability chronopotentiometric tests at a current density of 1000 mA cm$^{-2}$. (D) Illustration and SEM image of the graphite/carbon NPs/Cu/PTFE electrode. Long-term stability data of the modified polymer-based electrode for $CO_2$ reduction to ethylene in 7 M KOH. *Panels (A–C): Reproduced with permission from Y. Liu, et al., Corrosion engineering towards efficient oxygen evolution electrodes with stable catalytic activity for over 6000 hours, Nat. Commun. 9 (2018) 2609. Copyright © Springer Nature 2018. Panel (D): Reproduced with permission from C.-T. Dinh, et al., $CO_2$ electroreduction to ethylene via hydroxide-mediated copper catalysis at an abrupt interface, Science 360 (2018) 783–787. Copyright © 2018, American Association for the Advancement of Science.*

## 5.2 Catalyst degradation and the mitigation strategies

An important catalyst requirement is stability against corrosion under catalytic conditions. The chemical and physical stability of metallic catalysts vary with electrolyte pH. Some TM, TMO, and TMH heterogeneous catalysts operate well in alkaline media but are unstable in acidic media. For example, Ni catalysts used in commercial alkaline electrolyzers readily dissolve in acid. This corrosion issue can be suppressed by combining Ni with phosphorous to form amorphous alloys [153]. The corrosion resistance of Ni in acid is found to be improved with higher phosphorus content. Likewise, metal chalcogenide and carbide HER catalysts have greater stability in acidic electrolytes. A range of bimetallic HER catalysts are stable in alkaline electrolytes. CRR catalysts, such as Co, Ni, and Sn, operate in neutral and alkaline electrolytes. Pourbaix diagrams offer invaluable insights on the pH dependence of catalysts under applied potentials [154].

Catalyst degradation, in terms of efficiency or product selectivity, can be caused by physical changes, such as agglomeration or pulverization, either of which can decrease the availability of active sites and increase catalyst layer resistivity. Modification of the catalyst structure, such as nanostructuring, can enhance its physical stability. For example, 2D nanosheets can be fabricated as mechanically robust free-standing films; these have been shown to prevent catalyst agglomeration and detachment from their substrates [155]. Liu et al. reported that nanosheet arrays of layered double hydroxides exhibit good OER activity for more than 6000 h at $1\,\mathrm{A\,cm^{-2}}$ (see Fig. 7C) [156]. Other strategies include alteration of catalyst electronic properties by alloying [157], catalyst/support [158], and core-shell structures [159], all of which have been used to improve catalyst stability; in some cases, these changes can also enhance catalyst activity by modifying the binding energy of reaction intermediates.

Catalyst stability also depends on the mass transfer efficiency of reactant and products. In all OER, HER, and CRR reactions, substantial gas bubbles will form when operating at the high current densities. These temporarily block active sites, resulting in the loss of an overall catalytic activity. Mass transfer is strongly influenced by the catalyst wettability, thus modifications of surface hydrophobicity and hydrophilicity designed to improve compatibility with the liquid reactants can improve performance [160]. For example, Zhao and coworkers reported the enhancement of surface wettability by functionalization with highly hydrophilic borate [161] and phosphate [125] on Fe-based catalysts to promote dissipation of $O_2$ gas; the result was enhanced OER performance and catalyst stability at high current densities.

Gas diffusion electrodes (GDE) have gas-liquid-solid interfaces that afford efficient mass transfer of reactants and products to and from the catalyst surface. As shown in Fig. 7D, Sargent and coworkers prepared a durable GDE by applying coatings of carbon nanoparticles and graphite on a copper catalyst layer sputtered onto a porous PTFE support [64]. They proposed that the additional carbon support-coated layers stabilized the electrode surface by maintaining an abrupt reaction interface and ensuring even current distribution over the catalyst layer. The operational stability was evidenced by a constant ethylene faradaic efficiency (70%) for 150 h in 7 M KOH at −0.55 V vs RHE.

While physical changes of catalysts are usually irreversible, some chemical changes deleterious to catalyst performance are not. Catalyst poisoning is a common example. Noble metal catalysts, such as platinum, are susceptible to CO poisoning. Palladium catalysts are also poisoned by this $CO_2$ reduction product, but the effect is reversible upon removal of adsorbed CO on the catalyst surface [4]. For the Earth-abundant Ni, Fe, and Co catalysts, it was found a high CO* to H* coverage ratio at CRR operating potentials leads to CO poisoning that affects the product selectivity; it is proposed that CO* may block the surface and prevent C–H bond formation if the preceding reduction steps are kinetically facile [162].

Electrolyte purity can also have a significant impact on catalyst durability, as the presence of trace metals or organic impurities can be detrimental to electrocatalytic performance. For example, it was found that adventitious nickel present in buffered electrolytes gave OER current densities of $\sim 1\,\mathrm{mA\,cm^{-2}}$ in the absence of a catalyst at an overpotential of 400 mV [163]. Hori and coworkers reported the deposition of trace metal ions, suggested to be $Fe^{2+}$ and $Zn^{2+}$, as well as trimethylamine, was found to dramatically decrease the CRR performance of a copper-based heterogeneous catalyst [164]. To overcome this issue, several strategies have been employed, including pulsed-oxidative cycling of the electrode to remove of adsorbed organics [165], electrolyte preelectrolysis [164], and the use of ethylenediaminetetraacetic acid or a cation-exchange resin [166] to scavenge trace metal ion impurities.

## 6 Sustainability of electrocatalytic technologies

Most research into Earth-abundant catalysts for renewable energy conversion technology is appropriately focused on the development of systems with desirable operational characteristics. Often overlooked, however, are issues that will necessarily be important for widespread implementation of such systems, such as the environmental impacts of catalyst production and the need to safely dispose of or, better yet, recycle spent catalysts. This section examines how such issues have been framed in the relevant literature to date.

## 6.1 Life-cycle analysis

The sustainability of technologies driven by solar or other renewable energy sources is the subject of ongoing and increasingly sophisticated analytical tools. Life-cycle analysis has been developed to quantify not just the technical feasibility of such technologies but also their impact on the environment, including impacts from their production and their normal use [167, 168]. For example, when considering the use of photovoltaic solar panels for the generation of electricity, the manufacture of the panels is included along with their day-to-day operation to estimate their total environmental impacts. This approach, while capable of providing a useful overview of the many dimensions that need to be considered in the evaluation of the total impact of a given technology, is often too broad in scope to consider the impact that different catalysts may have on a given technology. As such, the relative advantages of shifting from a platinum group metal (PGM) catalyst to an Earth-abundant catalyst may not appear to have a significant impact in the analysis but, in practice, may have a large impact on the large-scale viability of new technologies. Nevertheless, it is worth noting that with respect to climate change considerations and other environmental impacts, water-splitting technologies, especially when driven by wind or hydropower, rank among the most environmentally friendly approaches to hydrogen production.

## 6.2 End-of-life technologies

Critical to the design of a closed-loop, or zero-waste, economy, is the ability to reclaim the material inputs for energy production. In the context of the current work, the fate of electrocatalysts is particularly germane. A recent survey of end-of-life technologies for electrocatalysts relevant to hydrogen production focused on the currently used PGM catalysts, for the obvious reason that these are, by far, the most widely used catalysts for a variety of water electrolysis processes, including alkaline electrolysis and proton-exchange water electrolyzers.

The most important approaches to reclaiming electrocatalysts that are currently used are hydrometallurgical, pyrometallurgical, and hydrothermal techniques. The first two involve leaching spent catalysts with appropriate acids to reclaim the metal ions (usually PGM ions), with the primary difference being an initial high temperature calcification step in the pyrometallurgical approach. These techniques can be readily modified to reclaim Earth-abundant metals as has recently been demonstrated for nickel catalysts [169].

There are a number of novel approaches to catalyst reclamation that avoid some of the hazardous or energy-intensive steps of the traditional techniques previously listed [170]. Several of these employ selective dissolution of metal ions, induced by either an applied potential, known as selective electrochemical dissolution [171], or by cycling through oxidizing and reducing environments by the introduction of $O_3$ and CO, respectively, known as transient dissolution [172]. These approaches have the added benefit of facilitating the recovery of catalyst supports and other components of the cell assemblies to which the catalyst materials may be adhered. Similar advantages have been demonstrated in another alternative to catalyst recovery, the alcohol solvent process [173]. This process employs a solvent-leaching step and microwave heating to promote delamination of polymer supports; the method has the potential to be a useful approach toward sustainable catalyst design provided issues around solvent recovery and reuse are overcome.

As is the case for the traditional approaches to catalyst recovery, the previously mentioned methods have been developed with PGM catalysts in mind. That said, the chemistry involved with the dissolution of metal ions and separation from support materials can be developed as part of a systems approach to catalyst design using Earth-abundant catalysts. Specifically, the ultimate recovery of the catalyst can be addressed as an integral aspect of the design of any catalytic system that will be employed on an industrial scale. Finally, as a practical matter, the development of catalyst recovery centers, which would facilitate the reclamation of catalysts employed by various facilities as part of closed-loop industrial processes, has been discussed [170].

## 7 Outlook

The development and utilization of low-cost Earth-abundant elements as high-performance electrocatalysts offers the promise of affordable, scalable, and sustainable electrochemical conversion technologies. Over the past 10 years, several Earth-abundant catalyst candidates have emerged that perform comparably to those based on noble metals. For example, Ni/Fe and $Ni_2P$ are excellent catalysts for OER and HER, respectively. There is also a range of efficient bifunctional water-splitting catalysts. Earth-abundant catalysts also have promise for CRR, especially as copper is an outstanding catalyst capable of synthesizing $C_{2+}$ products. Tin, zinc, and other bimetallic Earth-abundant catalysts effectively catalyze formate and CO production. However, much remains to be done to elucidate mechanistic details involving the electrode–electrolyte interface, requiring both experimental and theoretical studies. There are also significant gaps in understanding catalyst degradation mechanisms. These fundamental aspects of catalyst performance will be critical to develop rational strategies to improve overall performance by designing structures that will possess active sites, optimize the mass transfer of reactants and products, and improve stability. The development of in situ analytical techniques will certainly assist in this quest [174]. Overcoming those challenges, and coupling with an optimal electrochemical cell design, may lead to the successful implementation of durable and scalable Earth-abundant catalysts that are highly efficient and selective. Finally, advances in strategies to recycle and reclaim the used electrocatalysts will further the development of a sustainable economy. In a broader perspective, activities based on decarbonization have been accelerated in recent years. Hence, the future outlook in advancing electrochemical clean energy technologies on a large scale is highly promising. Advances in catalyst as described here will be critical to the deployment of future commercial electrolyzers.

## References

[1] H.S. Baker, et al., Higher $CO_2$ concentrations increase extreme event risk in a 1.5 °C world, Nat. Clim. Chang. 8 (2018) 604–608.

[2] J. Rogelj, et al., A new scenario logic for the Paris agreement long-term temperature goal, Nature 573 (2019) 357–363.

[3] M.G. Walter, et al., Solar water splitting cells, Chem. Rev. 110 (2010) 6446–6473.

[4] X. Min, M.W. Kanan, Pd-catalyzed electrohydrogenation of carbon dioxide to formate: high mass activity at low overpotential and identification of the deactivation pathway, J. Am. Chem. Soc. 137 (2015) 4701–4708.

[5] A.M. Appel, et al., Frontiers, opportunities, and challenges in biochemical and chemical catalysis of $CO_2$ fixation, Chem. Rev. 113 (2013) 6621–6658.

[6] K.J. Vetter, Electrochemical Kinetics: Theoretical Aspects, Academic Press, New York, 1967.

[7] S. Nitopi, et al., Progress and perspectives of electrochemical $CO_2$ reduction on copper in aqueous electrolyte, Chem. Rev. 119 (2019) 7610–7672.

[8] C. Xie, Z. Niu, D. Kim, M. Li, P. Yang, Surface and interface control in nanoparticle catalysis, Chem. Rev. 120 (2020) 1184–1249.

[9] Y. Li, et al., Recent advances on water-splitting electrocatalysis mediated by Noble-metal-based nanostructured materials, Adv. Energy Mater. 10 (2020) 1903120.

[10] Y. Hori, Electrochemical $CO_2$ reduction on metal electrodes, in: C.G. Vayenas, R.E. White, M.E. Gamboa-Aldeco (Eds.), Modern Aspects of Electrochemistry, Springer New York, New York, NY, 2008, pp. 89–189.

[11] G.B. Haxel, J.B. Hedrick, G.J. Orris, Rare earth elements—critical resources for high technology, in: U.S. Geological Survey Fact Sheet 087-02, 2002.

[12] H. Jin, et al., Emerging two-dimensional nanomaterials for electrocatalysis, Chem. Rev. 118 (2018) 6337–6408.

[13] Q. Yun, Q. Lu, X. Zhang, C. Tan, H. Zhang, Three-dimensional architectures constructed from transition-metal dichalcogenide nanomaterials for electrochemical energy storage and conversion, Angew. Chem. Int. Ed. 57 (2018) 626–646.

[14] C.-Y. Lee, J. Zou, J. Bullock, G.G. Wallace, Emerging approach in semiconductor photocatalysis: towards 3D architectures for efficient solar fuels generation in semi-artificial photosynthetic systems, J. Photochem. Photobiol. C 39 (2019) 142–160.

[15] B.M. Hunter, H.B. Gray, A.M. Müller, Earth-abundant heterogeneous water oxidation catalysts, Chem. Rev. 116 (2016) 14120–14136.

[16] Z.W. Seh, J. Kibsgaard, C.F. Dickens, I. Chorkendorff, J.K. Nørskov, T.F. Jaramillo, Combining theory and experiment in electrocatalysis: insights into materials design, Science 355 (2017), eaad4998.

[17] L. Trotochaud, S.L. Young, J.K. Ranney, S.W. Boettcher, Nickel–iron oxyhydroxide oxygen-evolution electrocatalysts: the role of intentional and incidental iron incorporation, J. Am. Chem. Soc. 136 (2014) 6744–6753.

[18] D.A. Corrigan, The catalysis of the oxygen evolution reaction by iron impurities in thin film nickel oxide electrodes, J. Electrochem. Soc. 134 (1987) 377.

[19] D. Friebel, et al., Identification of highly active fe sites in (Ni,Fe)OOH for electrocatalytic water splitting, J. Am. Chem. Soc. 137 (2015) 1305–1313.

[20] M.W. Louie, A.T. Bell, An investigation of thin-film Ni–Fe oxide catalysts for the electrochemical evolution of oxygen, J. Am. Chem. Soc. 135 (2013) 12329–12337.

[21] M. Gong, et al., An advanced Ni–Fe layered double hydroxide electrocatalyst for water oxidation, J. Am. Chem. Soc. 135 (2013) 8452–8455.

[22] W. Zhang, D. Li, L. Zhang, X. She, D. Yang, NiFe-based nanostructures on nickel foam as highly efficiently electrocatalysts for oxygen and hydrogen evolution reactions, J. Energy Chem. 39 (2019) 39–53.

[23] F. Song, et al., An unconventional iron nickel catalyst for the oxygen evolution reaction, ACS Central Sci. 5 (2019) 558–568.

[24] M. Gao, et al., Efficient water oxidation using nanostructured α-nickel-hydroxide as an electrocatalyst, J. Am. Chem. Soc. 136 (2014) 7077–7084.

[25] F. Lyu, Y. Bai, Q. Wang, L. Wang, X. Zhang, Y. Yin, Phase-controllable synthesis of cobalt hydroxide for electrocatalytic oxygen evolution, Dalton Trans. 46 (2017) 10545–10548.

[26] R. Brimblecombe, A. Koo, G.C. Dismukes, G.F. Swiegers, L. Spiccia, Solar driven water oxidation by a bioinspired manganese molecular catalyst, J. Am. Chem. Soc. 132 (2010) 2892–2894.

[27] K.N. Ferreira, T.M. Iverson, K. Maghlaoui, J. Barber, S. Iwata, Architecture of the photosynthetic oxygen-evolving center, Science 303 (2004) 1831–1838.

[28] I. Zaharieva, et al., Electrosynthesis, functional, and structural characterization of a water-oxidizing manganese oxide, Energy Environ. Sci. 5 (2012) 7081–7089.

[29] G. Mattioli, I. Zaharieva, H. Dau, L. Guidoni, Atomistic texture of amorphous manganese oxides for electrochemical water splitting revealed by ab initio calculations combined with X-ray spectroscopy, J. Am. Chem. Soc. 137 (2015) 10254–10267.

[30] Y. Gorlin, et al., In situ X-ray absorption spectroscopy investigation of a bifunctional manganese oxide catalyst with high activity for electrochemical water oxidation and oxygen reduction, J. Am. Chem. Soc. 135 (2013) 8525–8534.

[31] A. Ramírez, P. Hillebrand, D. Stellmach, M.M. May, P. Bogdanoff, S. Fiechter, Evaluation of MnOx, $Mn_2O_3$, and $Mn_3O_4$ electrodeposited films for the oxygen evolution reaction of water, J. Phys. Chem. C 118 (2014) 14073–14081.

[32] F. Zhou, A. Izgorodin, R.K. Hocking, L. Spiccia, D.R. MacFarlane, Electrodeposited MnOx films from ionic liquid for electrocatalytic water oxidation, Adv. Energy Mater. 2 (2012) 1013–1021.

[33] M.W. Kanan, D.G. Nocera, In situ formation of an oxygen-evolving catalyst in neutral water containing phosphate and $Co^{2+}$, Science 321 (2008) 1072–1075.

[34] D.A. Lutterman, Y. Surendranath, D.G. Nocera, A self-healing oxygen-evolving catalyst, J. Am. Chem. Soc. 131 (2009) 3838–3839.

[35] Y. Surendranath, M.W. Kanan, D.G. Nocera, Mechanistic studies of the oxygen evolution reaction by a cobalt-phosphate catalyst at neutral pH, J. Am. Chem. Soc. 132 (2010) 16501–16509.

[36] A.J. Esswein, Y. Surendranath, S.Y. Reece, D.G. Nocera, Highly active cobalt phosphate and borate based oxygen evolving catalysts operating in neutral and natural waters, Energy Environ. Sci. 4 (2011) 499–504.

[37] M. Dincă, Y. Surendranath, D.G. Nocera, Nickel-borate oxygen-evolving catalyst that functions under benign conditions, Proc. Natl. Acad. Sci. U. S. A. 107 (2010) 10337–10341.

[38] D.K. Bediako, B. Lassalle-Kaiser, Y. Surendranath, J. Yano, V.K. Yachandra, D.G. Nocera, Structure–activity correlations in a nickel–borate oxygen evolution catalyst, J. Am. Chem. Soc. 134 (2012) 6801–6809.

[39] D.K. Bediako, Y. Surendranath, D.G. Nocera, Mechanistic studies of the oxygen evolution reaction mediated by a nickel–borate thin film electrocatalyst, J. Am. Chem. Soc. 135 (2013) 3662–3674.

[40] M.H. Miles, Periodic variations of overvoltages for water electrolysis in acid solutions from cyclic voltammetric studies, J. Electrochem. Soc. 123 (1976) 1459.

[41] S.H. Ahn, et al., Electrodeposited Ni dendrites with high activity and durability for hydrogen evolution reaction in alkaline water electrolysis, J. Mater. Chem. 22 (2012) 15153–15159.

[42] H.J. Qiu, et al., Nanoporous graphene with single-atom nickel dopants: an efficient and stable catalyst for electrochemical hydrogen production (in eng), Angew. Chem. Int. Ed. 54 (2015) 14031–14035.

[43] J. Zhang, et al., Efficient hydrogen production on $MoNi_4$ electrocatalysts with fast water dissociation kinetics, Nat. Commun. 8 (2017) 15437.

[44] X. Wen, X. Yang, M. Li, L. Bai, J. Guan, Co/CoOx nanoparticles inlaid onto nitrogen-doped carbon-graphene as a trifunctional electrocatalyst, Electrochim. Acta 296 (2019) 830–841.

[45] Y. Jin, et al., Porous $MoO_2$ nanosheets as non-noble bifunctional electrocatalysts for overall water splitting, Adv. Mater. 28 (2016) 3785–3790.

[46] Y. Zhao, et al., Defect-engineered ultrathin δ-$MnO_2$ nanosheet arrays as bifunctional electrodes for efficient overall water splitting, Adv. Energy Mater. 7 (2017) 1700005.

[47] J. Chen, et al., $WO_3$–x nanoplates grown on carbon nanofibers for an efficient electrocatalytic hydrogen evolution reaction, ACS Appl. Mater. Inter. 8 (2016) 18132–18139.

[48] R. Wu, J. Zhang, Y. Shi, D. Liu, B. Zhang, Metallic $WO_2$–carbon mesoporous nanowires as highly efficient electrocatalysts for hydrogen evolution reaction, J. Am. Chem. Soc. 137 (2015) 6983–6986.

[49] R. Elakkiya, R. Ramkumar, G. Maduraiveeran, Flower-like nickel-cobalt oxide nanomaterials as bi-functional catalyst for electrochemical water splitting, Mater. Res. Bull. 116 (2019) 98–105.

[50] Y. Xu, et al., Supercritical $CO_2$-assisted synthesis of $NiFe_2O_4$/vertically-aligned carbon nanotube arrays hybrid as a bifunctional electrocatalyst for efficient overall water splitting, Carbon 145 (2019) 201–208.

[51] H. Wang, et al., Bifunctional non-noble metal oxide nanoparticle electrocatalysts through lithium-induced conversion for overall water splitting, Nat. Commun. 6 (2015) 7261.

[52] A. Bagger, W. Ju, A.S. Varela, P. Strasser, J. Rossmeisl, Electrochemical $CO_2$ reduction: a classification problem, ChemPhysChem 18 (2017) 3266–3273.

[53] Y. Hori, A. Murata, R. Takahashi, Formation of hydrocarbons in the electrochemical reduction of carbon dioxide at a copper electrode in aqueous solution, J. Chem. Soc. Faraday Trans. 85 (1989) 2309–2326.

[54] S. Gao, et al., Ultrathin $Co_3O_4$ layers realizing optimized $CO_2$ electroreduction to formate, Angew. Chem. Int. Ed. 55 (2016) 698–702.

[55] S. Gao, et al., Partially oxidized atomic cobalt layers for carbon dioxide electroreduction to liquid fuel, Nature 529 (2016) 68–71.

[56] K. Jiang, H. Wang, W.-B. Cai, H. Wang, Li electrochemical tuning of metal oxide for highly selective $CO_2$ reduction, ACS Nano 11 (2017) 6451–6458.

[57] W. Luo, J. Zhang, M. Li, A. Züttel, Boosting CO production in electrocatalytic $CO_2$ reduction on highly porous Zn catalysts, ACS Catal. 9 (2019) 3783–3791.

[58] Y. Hori, R. Takahashi, Y. Yoshinami, A. Murata, Electrochemical reduction of CO at a copper electrode, J. Phys. Chem. B 101 (1997) 7075–7081.

[59] C.W. Li, M.W. Kanan, $CO_2$ reduction at low Overpotential on cu electrodes resulting from the reduction of thick $Cu_2O$ films, J. Am. Chem. Soc. 134 (2012) 7231–7234.

[60] H. Mistry, et al., Highly selective plasma-activated copper catalysts for carbon dioxide reduction to ethylene, Nat. Commun. 7 (2016) 12123.

[61] A.D. Handoko, K.W. Chan, B.S. Yeo, $–CH_3$ mediated pathway for the electroreduction of $CO_2$ to ethane and ethanol on thick oxide-derived copper catalysts at low overpotentials, ACS Energy Lett. 2 (2017) 2103–2109.

[62] S. Lee, D. Kim, J. Lee, Electrocatalytic production of C3-C4 compounds by conversion of $CO_2$ on a chloride-induced bi-phasic $Cu_2O$-Cu catalyst, Angew. Chem. Int. Ed. 54 (2015) 14701–14705.

[63] T. Burdyny, W.A. Smith, $CO_2$ reduction on gas-diffusion electrodes and why catalytic performance must be assessed at commercially-relevant conditions, Energy Environ. Sci. 12 (2019) 1442–1453.

[64] C.-T. Dinh, et al., $CO_2$ electroreduction to ethylene via hydroxide-mediated copper catalysis at an abrupt interface, Science 360 (2018) 783–787.

[65] B. Hinnemann, et al., Biomimetic hydrogen evolution: $MoS_2$ nanoparticles as catalyst for hydrogen evolution, J. Am. Chem. Soc. 127 (2005) 5308–5309.

[66] T.F. Jaramillo, K.P. Jørgensen, J. Bonde, J.H. Nielsen, S. Horch, I. Chorkendorff, Identification of active edge sites for electrochemical $H_2$ evolution from $MoS_2$ nanocatalysts, Science 317 (2007) 100–102.

[67] C. Di Giovanni, et al., Bioinspired Iron sulfide nanoparticles for cheap and long-lived electrocatalytic molecular hydrogen evolution in neutral water, ACS Catal. 4 (2014) 681–687.

[68] J. Xie, et al., Defect-rich $MoS_2$ ultrathin nanosheets with additional active edge sites for enhanced electrocatalytic hydrogen evolution, Adv. Mater. 25 (2013) 5807–5813.

[69] G. Ye, et al., Defects engineered monolayer $MoS_2$ for improved hydrogen evolution reaction, Nano Lett. 16 (2016) 1097–1103.

[70] C. Tsai, F. Abild-Pedersen, J.K. Nørskov, Tuning the $MoS_2$ edge-site activity for hydrogen evolution via support interactions, Nano Lett. 14 (2014) 1381–1387.

[71] Y. Tan, et al., Monolayer $MoS_2$ films supported by 3D nanoporous metals for high-efficiency electrocatalytic hydrogen production, Adv. Mater. 26 (2014) 8023–8028.

[72] Y.-C. Lin, D.O. Dumcenco, Y.-S. Huang, K. Suenaga, Atomic mechanism of the semiconducting-to-metallic phase transition in single-layered $MoS_2$, Nat. Nanotech. 9 (2014) 391–396.

[73] G. Gao, Y. Jiao, F. Ma, Y. Jiao, E. Waclawik, A. Du, Charge mediated semiconducting-to-metallic phase transition in molybdenum disulfide monolayer and hydrogen evolution reaction in new 1T′ phase, J. Phys. Chem. C 119 (2015) 13124–13128.

[74] Y. Yin, et al., Synergistic phase and disorder engineering in 1T-$MoSe_2$ nanosheets for enhanced hydrogen-evolution reaction, Adv. Mater. 29 (2017) 1700311.

[75] L. Najafi, et al., Engineered $MoSe_2$-based heterostructures for efficient electrochemical hydrogen evolution reaction, Adv. Energy Mater. 8 (2018) 1703212.

[76] M.A. Lukowski, et al., Highly active hydrogen evolution catalysis from metallic $WS_2$ nanosheets, Energy Environ. Sci. 7 (2014) 2608–2613.

[77] S. Peng, et al., Cobalt sulfide nanosheet/graphene/carbon nanotube nanocomposites as flexible electrodes for hydrogen evolution, Angew. Chem. Int. Ed. 53 (2014) 12594–12599.

[78] N. Jiang, Q. Tang, M. Sheng, B. You, D.-E. Jiang, Y. Sun, Nickel sulfides for electrocatalytic hydrogen evolution under alkaline conditions: a case study of crystalline NiS, $NiS_2$, and $Ni_3S_2$ nanoparticles, Catal. Sci. Techn. 6 (2016) 1077–1084.

[79] X. Zou, et al., In situ generation of bifunctional, efficient Fe-based catalysts from Mackinawite iron sulfide for water splitting, Chem 4 (2018) 1139–1152.

[80] M. Asadi, et al., Robust carbon dioxide reduction on molybdenum disulphide edges, Nat. Commun. 5 (2014) 4470.

[81] M. Asadi, et al., Nanostructured transition metal dichalcogenide electrocatalysts for $CO_2$ reduction in ionic liquid, Science 353 (2016) 467–470.

[82] P. Abbasi, et al., Tailoring the edge structure of molybdenum disulfide toward electrocatalytic reduction of carbon dioxide, ACS Nano 11 (2017) 453–460.

[83] J. Zhang, Y. Hu, D. Liu, Y. Yu, B. Zhang, Enhancing oxygen evolution reaction at high current densities on amorphous-like Ni–Fe–S ultrathin nanosheets via oxygen incorporation and electrochemical tuning, Adv. Sci. 4 (2017) 1600343.

[84] Y. Liu, et al., Low overpotential in vacancy-rich ultrathin $CoSe_2$ nanosheets for water oxidation, J. Am. Chem. Soc. 136 (2014) 15670–15675.

[85] A. Parra-Puerto, K.L. Ng, K. Fahy, A.E. Goode, M.P. Ryan, A. Kucernak, Supported transition metal phosphides: activity survey for HER, ORR, OER, and corrosion resistance in acid and alkaline electrolytes, ACS Catal. 9 (2019) 11515–11529.

[86] P. Liu, J.A. Rodriguez, Catalysts for hydrogen evolution from the [NiFe] hydrogenase to the $Ni_2P(001)$ surface: the importance of ensemble effect, J. Am. Chem. Soc. 127 (2005) 14871–14878.

[87] I. Paseka, Evolution of hydrogen and its sorption on remarkable active amorphous smooth Ni P(x) electrodes, Electrochim. Acta 40 (1995) 1633–1640.

[88] E.J. Popczun, et al., Nanostructured nickel phosphide as an electrocatalyst for the hydrogen evolution reaction, J. Am. Chem. Soc. 135 (2013) 9267–9270.

[89] E.J. Popczun, C.G. Read, C.W. Roske, N.S. Lewis, R.E. Schaak, Highly active electrocatalysis of the hydrogen evolution reaction by cobalt phosphide nanoparticles, Angew. Chem. Int. Ed. 53 (2014) 5427–5430.

[90] P. Jiang, Q. Liu, Y. Liang, J. Tian, A.M. Asiri, X. Sun, A cost-effective 3D hydrogen evolution cathode with high catalytic activity: FeP nanowire array as the active phase, Angew. Chem. Int. Ed. 53 (2014) 12855–12859.

[91] J. Kibsgaard, T.F. Jaramillo, Molybdenum phosphosulfide: an active, acid-stable, earth-abundant catalyst for the hydrogen evolution reaction, Angew. Chem. Int. Ed. 53 (2014) 14433–14437.

[92] X. Peng, C. Pi, X. Zhang, S. Li, K. Huo, P.K. Chu, Recent progress of transition metal nitrides for efficient electrocatalytic water splitting, Sustain. Energy Fuels 3 (2019) 366–381.

[93] W.-F. Chen, J.T. Muckerman, E. Fujita, Recent developments in transition metal carbides and nitrides as hydrogen evolution electrocatalysts, Chem. Commun. 49 (2013) 8896–8909.

[94] H.B. Aiyappa, J. Masa, C. Andronescu, M. Muhler, R.A. Fischer, W. Schuhmann, MOFs for electrocatalysis: from serendipity to design strategies, Small Meth. 3 (2019) 1800415.

[95] S. Zhao, et al., Ultrathin metal–organic framework nanosheets for electrocatalytic oxygen evolution, Nat. Energy 1 (2016) 16184.

[96] J. Duan, S. Chen, C. Zhao, Ultrathin metal-organic framework array for efficient electrocatalytic water splitting, Nat. Commun. 8 (2017) 15341.

[97] N. Kornienko, et al., Metal–organic frameworks for electrocatalytic reduction of carbon dioxide, J. Am. Chem. Soc. 137 (2015) 14129–14135.

[98] J.T. Feaster, et al., Understanding selectivity for the electrochemical reduction of carbon dioxide to formic acid and carbon monoxide on metal electrodes, ACS Catal. 7 (2017) 4822–4827.

[99] S. Zhang, P. Kang, T.J. Meyer, Nanostructured tin catalysts for selective electrochemical reduction of carbon dioxide to formate, J. Am. Chem. Soc. 136 (2014) 1734–1737.

[100] C. Liang, et al., High efficiency electrochemical reduction of $CO_2$ beyond the two-electron transfer pathway on grain boundary rich ultra-small $SnO_2$ nanoparticles, J. Mater. Chem. A 6 (2018) 10313–10319.

[101] C.W. Lee, et al., Selective electrochemical production of Formate from carbon dioxide with bismuth-based catalysts in an aqueous electrolyte, ACS Catal. 8 (2018) 931–937.

[102] H. Zhong, Y. Qiu, T. Zhang, X. Li, H. Zhang, X. Chen, Bismuth nanodendrites as a high performance electrocatalyst for selective conversion of $CO_2$ to formate, J. Mater. Chem. A 4 (2016) 13746–13753.

[103] S. Kim, et al., Shape-controlled bismuth nanoflakes as highly selective catalysts for electrochemical carbon dioxide reduction to formate, Nano Energy 39 (2017) 44–52.

[104] Q. Li, et al., Tuning Sn-catalysis for electrochemical reduction of $CO_2$ to CO via the Core/Shell Cu/$SnO_2$ structure, J. Am. Chem. Soc. 139 (2017) 4290–4293.

[105] G. Wen, et al., Orbital interactions in bi-Sn bimetallic electrocatalysts for highly selective electrochemical $CO_2$ reduction toward formate production, Adv. Energy Mater. 8 (2018) 1802427.

[106] K. Gong, F. Du, Z. Xia, M. Durstock, L. Dai, Nitrogen-doped carbon nanotube arrays with high electrocatalytic activity for oxygen reduction, Science 323 (2009) 760–764.

[107] K.S. Novoselov, et al., Electric field effect in atomically thin carbon films, Science 306 (2004) 666–669.

[108] D. Deng, K.S. Novoselov, Q. Fu, N. Zheng, Z. Tian, X. Bao, Catalysis with two-dimensional materials and their heterostructures, Nat. Nanotechnol. 11 (2016) 218–230.

[109] H. Wang, et al., Three-dimensional graphene networks with abundant sharp edge sites for efficient electrocatalytic hydrogen evolution, Angew. Chem. Int. Ed. 57 (2018) 192–197.

[110] Y. Ito, W. Cong, T. Fujita, Z. Tang, M. Chen, High catalytic activity of nitrogen and sulfur co-doped nanoporous graphene in the hydrogen evolution reaction, Angew. Chem. Int. Ed. 54 (2015) 2131–2136.

[111] Y. Jiao, Y. Zheng, K. Davey, S.-Z. Qiao, Activity origin and catalyst design principles for electrocatalytic hydrogen evolution on heteroatom-doped graphene, Nat. Energy 1 (2016) 16130.

[112] J. Wu, et al., Incorporation of nitrogen defects for efficient reduction of $CO_2$ via two-Electron pathway on three-dimensional graphene foam, Nano Lett. 16 (2016) 466–470.

[113] P.P. Sharma, et al., Nitrogen-doped carbon nanotube arrays for high-efficiency electrochemical reduction of $CO_2$: on the understanding of defects, defect density, and selectivity, Angew. Chem. Int. Ed. 54 (2015) 13701–13705.

[114] H. Wang, Y. Chen, X. Hou, C. Ma, T. Tan, Nitrogen-doped graphenes as efficient electrocatalysts for the selective reduction of carbon dioxide to formate in aqueous solution, Green Chem. 18 (2016) 3250–3256.

[115] Z. Hong, B. Shen, Y. Chen, B. Lin, B. Gao, Enhancement of photocatalytic H2 evolution over nitrogen-deficient graphitic carbon nitride, J. Mater. Chem. A 1 (2013) 11754–11761.

[116] V.W.-H. Lau, M.B. Mesch, V. Duppel, V. Blum, J. Senker, B.V. Lotsch, Low-molecular-weight carbon nitrides for solar hydrogen evolution, J. Am. Chem. Soc. 137 (2015) 1064–1072.

[117] D. Guo, R. Shibuya, C. Akiba, S. Saji, T. Kondo, J. Nakamura, Active sites of nitrogen-doped carbon materials for oxygen reduction reaction clarified using model catalysts, Science 351 (2016) 361–365.

[118] Y. Zheng, et al., Hydrogen evolution by a metal-free electrocatalyst, Nat. Commun. 5 (2014) 3783.

[119] Y. Jiao, Y. Zheng, P. Chen, M. Jaroniec, S.-Z. Qiao, Molecular scaffolding strategy with synergistic active centers to facilitate electrocatalytic $CO_2$ reduction to hydrocarbon/alcohol, J. Am. Chem. Soc. 139 (2017) 18093–18100.

[120] X. Lu, T.H. Tan, Y.H. Ng, R. Amal, Highly selective and stable reduction of $CO_2$ to CO by a graphitic carbon nitride/carbon nanotube composite electrocatalyst, Chem. A Euro. J. 22 (2016) 11991–11996.

[121] D. Gao, R. Liu, J. Biskupek, U. Kaiser, Y.-F. Song, C. Streb, Modular design of noble-metal-free mixed metal oxide electrocatalysts for complete water splitting, Angew. Chem. Int. Ed. 58 (2019) 4644–4648.

[122] J. Su, R. Ge, Y. Dong, F. Hao, L. Chen, Recent progress in single-atom electrocatalysts: concept, synthesis, and applications in clean energy conversion, J. Mater. Chem. A 6 (2018) 14025–14042.

[123] U.S. Mohanty, Electrodeposition: a versatile and inexpensive tool for the synthesis of nanoparticles, nanorods, nanowires, and nanoclusters of metals, J. Appl. Electrochem. 41 (2011) 257–270.

[124] C. Chen, Y. Pang, F. Zhang, J. Zhong, B. Zhang, Z. Cheng, Sharp Cu@Sn nanocones on cu foam for highly selective and efficient electrochemical reduction of $CO_2$ to formate, J. Mater. Chem. A 6 (2018) 19621–19630.

[125] Y. Li, C. Zhao, Enhancing water oxidation catalysis on a synergistic phosphorylated NiFe hydroxide by adjusting catalyst wettability, ACS Catal. 7 (2017) 2535–2541.

[126] X. Lu, C. Zhao, Electrodeposition of hierarchically structured three-dimensional nickel–iron electrodes for efficient oxygen evolution at high current densities, Nat. Commun. 6 (2015) 6616.

[127] M.W. Kanan, Y. Surendranath, D.G. Nocera, Cobalt–phosphate oxygen-evolving compound, Chem. Soc. Rev. 38 (2009) 109–114.

[128] C.-Y. Lee, K. Lee, P. Schmuki, Anodic formation of self-organized cobalt oxide nanoporous layers, Angew. Chem. Int. Ed. 52 (2013) 2077–2081.

[129] D. Gao, R.M. Arán-Ais, H.S. Jeon, B. Roldan Cuenya, Rational catalyst and electrolyte design for $CO_2$ electroreduction towards multicarbon products, Nat. Catal. 2 (2019) 198–210.

[130] S.Y. Lee, H. Jung, N.-K. Kim, H.-S. Oh, B.K. Min, Y.J. Hwang, Mixed copper states in anodized cu electrocatalyst for stable and selective ethylene production from $CO_2$ reduction, J. Am. Chem. Soc. 140 (2018) 8681–8689.

[131] Y. Chen, et al., Two-dimensional metal nanomaterials: synthesis, properties, and applications, Chem. Rev. 118 (2018) 6409–6455.

[132] M. Hujjatul Islam, M.T.Y. Paul, O.S. Burheim, B.G. Pollet, Recent developments in the sonoelectrochemical synthesis of nanomaterials, Ultrason. Sonochem. 59 (2019) 104711.

[133] F. Li, et al., N-doped carbon coated $NiCo_2S_4$ hollow nanotube as bifunctional electrocatalyst for overall water splitting, Carbon 145 (2019) 521–528.

[134] K. Wang, et al., Facile synthesis of nanoporous Ni–Fe–P bifunctional catalysts with high performance for overall water splitting, J. Mater. Chem. A 7 (2019) 2518–2523.

[135] H. Wang, T. Maiyalagan, X. Wang, Review on recent progress in nitrogen-doped graphene: synthesis, characterization, and its potential applications, ACS Catal. 2 (2012) 781–794.

[136] A.N. Gleizes, MOCVD of chalcogenides, pnictides, and heterometallic compounds from single-source molecule precursors, Chem. Vap. Depos. 6 (2000) 155–173.

[137] H. Mistry, A.S. Varela, S. Kühl, P. Strasser, B.R. Cuenya, Nanostructured electrocatalysts with tunable activity and selectivity, Nat. Rev. Mater. 1 (2016) 16009.

[138] C. Koenigsmann, S.S. Wong, One-dimensional noble metal electrocatalysts: a promising structural paradigm for direct methanol fuel cells, Energy Environ. Sci. 4 (2011) 1161–1176.

[139] R. Zhang, et al., Ternary $NiCo_2Px$ nanowires as pH-universal electrocatalysts for highly efficient hydrogen evolution reaction, Adv. Mater. 29 (2017) 1605502.

[140] O. Diaz-Morales, I. Ledezma-Yanez, M.T.M. Koper, F. Calle-Vallejo, Guidelines for the rational design of Ni-based double hydroxide electrocatalysts for the oxygen evolution reaction, ACS Catal. 5 (2015) 5380–5387.

[141] B. Zhang, et al., Interface engineering: the $Ni(OH)_2/MoS_2$ heterostructure for highly efficient alkaline hydrogen evolution, Nano Energy 37 (2017) 74–80.

[142] Q. Lu, et al., Highly porous non-precious bimetallic electrocatalysts for efficient hydrogen evolution, Nat. Commun. 6 (2015) 6567.

[143] Y. Sun, S. Gao, F. Lei, J. Liu, L. Liang, Y. Xie, Atomically-thin non-layered cobalt oxide porous sheets for highly efficient oxygen-evolving electrocatalysts, Chem. Sci. 5 (2014) 3976–3982.

[144] Y. Wang, et al., Reduced mesoporous $Co_3O_4$ nanowires as efficient water oxidation electrocatalysts and supercapacitor electrodes, Adv. Energy Mater. 4 (2014) 1400696.

[145] L. Liu, et al., Probing the crystal plane effect of $Co_3O_4$ for enhanced electrocatalytic performance toward efficient overall water splitting, ACS Appl. Mater. Inter. 9 (2017) 27736–27744.

[146] Y. Zhao, et al., Sub-3 nm ultrafine monolayer layered double hydroxide nanosheets for electrochemical water oxidation, Adv. Energy Mater. 8 (2018) 1703585.

[147] H. Li, et al., Activating and optimizing $MoS_2$ basal planes for hydrogen evolution through the formation of strained Sulphur vacancies, Nat. Mater. 15 (2016) 48–53.

[148] D. Voiry, et al., Conducting $MoS_2$ nanosheets as catalysts for hydrogen evolution reaction, Nano Lett. 13 (2013) 6222–6227.

[149] Z.W. Chen, L.X. Chen, Z. Wen, Q. Jiang, Understanding electro-catalysis by using density functional theory, Phys. Chem. Chem. Phys. 21 (2019) 23782–23802.

[150] K. Tran, Z.W. Ulissi, Active learning across intermetallics to guide discovery of electrocatalysts for $CO_2$ reduction and $H_2$ evolution, Nat. Catal. 1 (2018) 696–703.

[151] P. Aßmann, A.S. Gago, P. Gazdzicki, K.A. Friedrich, M. Wark, Toward developing accelerated stress tests for proton exchange membrane electrolyzers, Curr. Opin. Electrochem. 21 (2020) 225–233.

[152] D. Delgado, F. Bizzotto, A. Zana, M. Arenz, Accelerated durability test for high-surface-area oxyhydroxide nickel supported on Raney nickel as catalyst for the alkaline oxygen evolution reaction, ChemPhysChem 20 (2019) 3147–3153.

[153] A.R.J. Kucernak, V.N. Naranammalpuram Sundaram, Nickel phosphide: the effect of phosphorus content on hydrogen evolution activity and corrosion resistance in acidic medium, J. Mater. Chem. A 2 (2014) 17435–17445.

[154] T.J. O'Keeke, Pourbaix diagrams, in: K.H.J. Buschow, et al. (Eds.), Encyclopedia of Materials: Science and Technology, Elsevier, Oxford, 2001, pp. 7774–7781.

[155] C. Tan, et al., Recent advances in ultrathin two-dimensional nanomaterials, Chem. Rev. 117 (2017) 6225–6331.

[156] Y. Liu, et al., Corrosion engineering towards efficient oxygen evolution electrodes with stable catalytic activity for over 6000 hours, Nat. Commun. 9 (2018) 2609.

[157] Y.-T. Pan, H. Yang, Design of bimetallic catalysts and electrocatalysts through the control of reactive environments, Nano Today 31 (2020) 100832.

[158] H. Li, et al., Interfacial effects in supported catalysts for electrocatalysis, J. Mater. Chem. A 7 (2019) 23432–23450.

[159] S.T. Hunt, Y. Román-Leshkov, Principles and methods for the rational design of core–shell nanoparticle catalysts with ultralow Noble metal loadings, Acc. Chem. Res. 51 (2018) 1054–1062.

[160] L. Wang, F.-S. Xiao, The importance of catalyst wettability, ChemCatChem 6 (2014) 3048–3052.

[161] K. Dastafkan, Y. Li, Y. Zeng, L. Han, C. Zhao, Enhanced surface wettability and innate activity of an iron borate catalyst for efficient oxygen evolution and gas bubble detachment, J. Mater. Chem. A 7 (2019) 15252–15261.

[162] S.A. Akhade, W. Luo, X. Nie, N.J. Bernstein, A. Asthagiri, M.J. Janik, Poisoning effect of adsorbed CO during $CO_2$ electroreduction on late transition metals, Phys. Chem. Chem. Phys. 16 (2014) 20429–20435.

[163] I. Roger, M.D. Symes, Efficient electrocatalytic water oxidation at neutral and high pH by adventitious nickel at nanomolar concentrations, J. Am. Chem. Soc. 137 (2015) 13980–13988.

[164] Y. Hori, et al., "Deactivation of copper electrode" in electrochemical reduction of $CO_2$, Electrochim. Acta 50 (2005) 5354–5369.

[165] P. Kedzierzawski, Poisoning and activation of the gold cathode during electroreduction of $CO_2$, J. Electrochem. Soc. 141 (1994) L58.

[166] A. Wuttig, Y. Surendranath, Impurity ion complexation enhances carbon dioxide reduction catalysis, ACS Catal. 5 (2015) 4479–4484.

[167] A. Mehmeti, A. Angelis-Dimakis, G. Arampatzis, S.J. McPhail, S. Ulgiati, Life cycle assessment and water footprint of hydrogen production methods: from conventional to emerging technologies, Environments 5 (2018) 24.

[168] R. Bhandari, C.A. Trudewind, P. Zapp, Life cycle assessment of hydrogen production via electrolysis—a review, J. Cleaner Product. 85 (2014) 151–163.

[169] J.Y. Lee, S.V. Rao, B.N. Kumar, D.J. Kang, B.R. Reddy, Nickel recovery from spent Raney nickel catalyst through dilute sulfuric acid leaching and soda ash precipitation, J. Hazard. Mater. 176 (2010) 1122–1125.

[170] A. Valente, D. Iribarren, J. Dufour, End of life of fuel cells and hydrogen products: from technologies to strategies, Int. J. Hydrog. Energy 44 (2019) 20965–20977.

[171] R. Latsuzbaia, E. Negro, G.J.M. Koper, Environmentally friendly carbon-preserving recovery of Noble metals from supported fuel cell catalysts, ChemSusChem 8 (2015) 1926–1934.

[172] N. Hodnik, et al., Platinum recycling going green via induced surface potential alteration enabling fast and efficient dissolution, Nat. Commun. 7 (2016) 13164.

[173] L. Shore, Process for recycling components of a PEM fuel cell membrane electrode assembly. U.S. Patent No. 8,124,261, 2012.

[174] X. Li, S. Wang, L. Li, Y. Sun, Y. Xie, Progress and perspective for in situ studies of $CO_2$ reduction, J. Am. Chem. Soc. 142 (2020) 9567–9581.